The inhibitory microcircuit of the substantia nigra provides feedback gain control of the basal ganglia output

Jennifer Brown, Wei-Xing Pan, Joshua T Dudman

DOI: http://dx.doi.org/10.7554/eLife.02397

Cite as: eLife 2014;10.7554/eLife.02397

Received: 26 January 2014
Accepted: 17 May 2014
Published: 21 May 2014

The inhibitory microcircuit of the substantia nigra provides feedback gain control of the basal ganglia output

Jennifer Brown[1,2], Wei-Xing Pan[1], and Joshua Tate Dudman[1,*]

[1] Howard Hughes Medical Institute, Janelia Farm Research Campus, 19700 Helix Drive, Ashburn, VA 20147
[2] Department of Physiology, Development and Neuroscience, University of Cambridge, Downing Street, Cambridge, CB2 3DY, UK
[*] To whom correspondence should be addressed: dudmanj@janelia.hhmi.org

ABSTRACT

Dysfunction of the basal ganglia produces severe deficits in the timing, initiation, and vigor of movement. These diverse impairments suggest a control system gone awry. In engineered systems feedback is critical for control. By contrast, models of the basal ganglia highlight feed forward circuitry and ignore intrinsic feedback circuits. Here we show that feedback via axon collaterals of substantia nigra projection neurons control the gain of the basal ganglia output. Through a combination of physiology, optogenetics, anatomy and circuit mapping we elaborate a general circuit mechanism for gain control in a microcircuit lacking interneurons. Our data suggest that diverse tonic firing rates, weak unitary connections, and a spatially diffuse collateral circuit with distinct topography and kinetics from feed forward input is sufficient to implement divisive feedback inhibition. The importance of feedback for engineered systems implies that the intranigral microcircuit, despite its absence from canonical models, could be essential to basal ganglia function.

INTRODUCTION

The basal ganglia are a collection of interconnected subcortical regions of the vertebrate brain[1]. Pathological disruptions of basal ganglia signaling produce profound deficits in the timing[2], vigor[3], and initiation[4] of voluntary movements. While it is thus clear that the basal ganglia are critical for voluntary movement, the specific mechanisms by which movement is controlled by basal ganglia activity remain unclear [3]. Voluntary control of movement can be explained in terms of optimal feedback control theory[5]. The basal ganglia circuit can be described as an extended loop that begins with projections from deep layer cortical neurons and ultimately returns to the cortex via projections from the basal ganglia to the ventral thalamus [6]. However, the basal ganglia circuit also contains intrinsic feedback projections [7]. In engineered control systems, feedback is critical for stable performance[8].

The substantia nigra (SN) pars reticulata (SNr) is the primary source of output from the sensorimotor basal ganglia in rodents [7]. The vast majority of neurons in the SNr are projection neurons that synthesize and release the neurotransmitter □-aminobutryic acid (GABA). Projection neurons of the SNr target pre-motor areas in the ventral thalamus, dorsal midbrain and tegmentum[9,10]. In addition to these long range targets, nigral projection neurons also elaborate axon collaterals within the SN [11] [12,13]. There are no known interneurons in the SNr [12], and thus collaterals of projection neurons are the sole source of intrinsic feedback for the basal ganglia output. Anatomical reconstructions have indicated that the axon collaterals of SNr projection neurons are sparse[13]. The functional impact of this intranigral microcircuit remains unclear. Antidromic activation of SNr projection neurons in anesthetized animals has been used to infer the presence of inhibition via projection neurons collaterals[14,15]; however, the relative impact, spatial organization and temporal properties of recruitment of feedback inhibition via SNr collateral inhibition remains largely unknown. Here, we explore the hypothesis that the microcircuit formed by SNr collaterals could implement a critical negative feedback node in the context of a control system for voluntary behavior that is implemented in the extended cortico-basal ganglia circuit.

In engineered systems the functional impact of a negative feedback can be difficult to detect and characterize[8]. For example, at steady state or in the absence of change in the state of the system there may be no obvious effect of appropriately functioning negative feedback. However, sudden transitions in the state of the system can reveal the contribution of negative feedback – altering, for example, the gain and/or the time course of settling around transitions. By analogy to an engineered system the SNr microcircuit may have little apparent impact in the absence of sudden changes in the state of the population activity. However, changes in behavior and receipt of sensory stimuli are accompanied by phasic transitions, both increases and decreases, in the activity of the SNr population. We thus reasoned that the role of negative feedback, implemented by the SNr microcircuit, could become apparent under such conditions. Recent work has shown that a salient or conditioned stimulus (CS), for example an auditory tone, can lead to phasic changes in the activity of SNr neurons in rodents [16]. Moreover, these short-latency modulations of activity are predictive of the initiation of conditioned behavioral responses – *i.e.* action selection [16,17]. If the basal ganglia acts as a control system for behavior, then we would predict that control over the gain or dynamic range of these phasic modulations should be critical for normal voluntary actions.

Detailed study of the local inhibitory connections within the SNr has been hampered by the difficulty in isolating and specifically exciting the SNr collaterals independent of afferent inhibitory and excitatory projections[18]. We overcame this challenge by using cell-type specific expression of channelrhodopsin-2 (ChR2), a light gated cation channel [19,20], in SNr GABA neurons. This optogenetic approach allowed us to stimulate SNr GABA neurons with high temporal and spatial resolution without contamination from excitatory afferents, dopaminergic transmission, or afferent inhibitory input from the striatonigral projection both *in vitro* and *in vivo*.

Consistent with the prediction from anatomical data we show that inhibition derived from the collaterals of projection neurons in the SNr is sparse and has little to no effect on tonic baseline firing. However, we also observed that activation of the SNr projection neuron population could elicit a large and potent feedback inhibition capable of shaping output activity. Here we show that this unique combination of effects is the result of a number of distinctive features of the SN microcircuit: 1) postsynaptic currents resulting from collateral synaptic input provided robust inhibition with a rapid onset during strong activation of the network; 2) unitary connections are weak with sufficiently low release probability to sustain release during repetitive stimulation; 3) asynchronous basal inhibition in the tonically active network is effectively compensated for by intrinsic conductances that sustain tonic spiking; 4) the potency of feedback inhibition is proportional to total activation of the microcircuit due to a sparse, spatially diffuse connectivity. Together, these properties of the intrinsic microcircuit of the SNr implement a robust inhibition that is rapidly and stably recruited in proportion to the sustained activation of the projection neuron population with little effect in the absence of stimulation – in other words, the inhibitory microcircuit of the SNr mediates a divisive gain control on the basal ganglia output.

RESULTS

If collateral, feedback projections of SNr neurons provides a source of negative feedback, then we would expect that the level of activation of the population immediately prior to a stimulus should be inversely correlated with the modulation of the response of an individual neuron to that stimulus. In other words, if there were more activity producing collateral inhibition the phasic response to a stimulus could be blunted. To test this possibility we examined a dataset of 599 single units recorded from the ventral midbrain of mice (*n* = 5, strongly biased towards recordings from GABAergic neurons in the SN, see Methods) performing a classical trace conditioning task described previously [17]. For each individual unit we computed the normalized response to a salient stimulus (an auditory tone that predicted a delayed reward) as a function of the normalized activity of the simultaneously recorded population of neurons for 32 recording sessions in which at least 8 neurons were recorded simultaneously (median = 12; maximum = 21) for each trial in the recording session (median = 71 trials; range = 42:132) (Figure 1a-b). This yielded a dataset of 28,277 comparisons from which we estimated the correlation between the activation of the population at baseline to the activation of each individual neuron in response to the conditioned stimulus (CS). We found that both the population (-0.1; $p<0.001$ permutation test) and 22/32 individual sessions exhibited significant negative correlations (-0.12 ± 0.05 s.d.; $p<0.05$, permutation test; (Figure 1c)).

These data thus suggest that the activation of the SNr population indeed provides a negative feedback to limit the phasic response of the population to salient stimuli. However, these data also imply a surprising structure to the SNr microcircuit – namely, even a relatively poor estimate of population activity (7-20 simultaneously recorded units across electrodes spread over hundreds of microns) is sufficient to provide predictive power for the response of individual units. However, significant individual pairwise correlations were very rarely observed in these recordings[17] consistent with prior work[21]. This would suggest that either the negative correlation observed is a consequence of correlations in activity due to extended feedback projections or that individual units receive relatively weak and diffuse input from many SN neurons rather than strong feedback inhibition from proximally located neurons.

To distinguish between these possibilities we first sought to test whether this negative feedback property of the SN microcircuit could be recapitulated in an *in vitro* preparation where extrinsic, multisynaptic sources of feedback are eliminated. The functional properties of feedback inhibition to the basal ganglia were assessed by channelrhodopsin-2 (ChR2) mediated stimulation of SNr GABA neurons. In one set of experiments an adeno-associated virus (AAV) that expressed a *cre*-dependent ChR2 transgene [22] was injected into the SNr of a mouse line in which *cre*-recombinase was expressed under the glutamic acid decarboxylase (*Gad2*) promoter to target expression to SNr GABA neurons (hereafter referred to as *Gad2*-ChR2; Figure 2a,c). In the other we exploited a transgenic mouse line which has strong expression of ChR2 under the control of the thymus cell antigen 1 (*Thy1*) promoter [23], (hereafter referred to as *Thy1*-ChR2; Figure 2b,d). In this transgenic line ChR2 is robustly expressed in SNr GABA neurons, but not in SN dopaminergic neurons[17] or in upstream projection neurons of the dorsal striatum[24]. Both approaches thus provide a method to specifically excite SNr GABA neurons with high reliability and fine temporal resolution (Figure 2e-j).

Local SNr inhibition is sufficient to modify basal ganglia output during phasic activation

Local axon collaterals of projection neurons provide a source of feedback inhibition proportional to the output of the SNr. For this inhibition to regulate the output of the SNr it must be sufficient to suppress activity even in the presence of strong, phasic activation of projection neurons. Phasic activation of the SNr population occurs, for example, at the onset of salient sensory cues [25 17] (Figure 3–figure supplemental 1). Thus, to determine whether local inhibition was sufficient to regulate the gain of the SNr network, we used ChR2 stimulation to drive repetitive somatic spiking in the projection neuron network. This recruits a population of SNr neurons with a time course and distribution of responses similar to that evoked by conditioned stimuli (ref. [17], Figure 3–figure supplemental 1). We determined the consequences of local inhibition by comparing activity evoked when inhibition was intact with activity evoked following pharmacological blockade of inhibition.

Whole cell current-clamp recordings from individual SNr projection neurons where obtained from brain slices of *Thy1*-ChR2 mice in the presence of excitatory synaptic transmission blockers (D-AP5 and NBQX; Figure 3a). Wide-field illumination through a 10X objective was used to stimulate activity throughout the SNr network. Direct light-evoked spiking in the recorded neuron was substantially, or in some cases completely, suppressed under control conditions (Figure 3b-c). However, reliable light-evoked spiking was always present following application of the $GABA_A$ receptor antagonist gabazine (Gbz) to block local inhibition (Figure 3d). The suppression of evoked spiking was consistent across stimulus durations within a cell (Figure 3e), whereas the magnitude of suppression was more idiosyncratic across cells for a given stimulus condition (Figure 3f).

The ability of feedback inhibition to suppress spiking more effectively with increasing stimulus duration (Figure 3e) implies a divisive gain control. To quantify the gain effect across the population we compared the normalized response to photostimulation of increasing duration both in the presence and absence of inhibitory synaptic transmission (Figure 3g). We found that the response of the population showed a significant increase as a function of stimulus duration and the magnitude of the increase was significantly reduced by the presence of feedback inhibition (two-factor ANOVA; $p<0.05$). Divisive gain control is characterized by a suppression of spiking at large stimuli but little to no effect on the response to weak or absent stimuli. Consistent with a divisive gain control we found that baseline firing was unaffected by removal of inhibition (Figure 3g, open circles). To contrast a feedback gain control with the effect predicted for subtractive inhibition we examined recordings from dopamine neurons of the SN that do not express ChR2, but are strongly inhibited by ChR2 expressing projection neurons[17]. For dopamine neurons we observed a constant suppression of spiking across the range of stimuli used (also see ref [17]). If the reduction in spiking observed during stimulation was the result of feedback inhibition one would predict that the inhibition should onset after the onset of the population response and truncate the response present in the absence of feedback. Consistent with this prediction we found that suppression of spiking was characterized by a significant decrease in the duration of the evoked spiking (Figure 3h). This effect on the duration could be observed in many individual neuron responses (Figure 3f).

Our *in vivo* results suggested that the extent of suppression of transient activation in SNr neurons is proportional to the estimated activation of the network (Figure 1). Anatomical studies indicate that the vast majority of projection neurons elaborate collaterals within the SNr, however, these collaterals can form relatively few (~10) putative synaptic contacts[13]. Moreover, we found that unitary release events produced relatively weak mIPSCs (~150 pS) (Figure 3-figure

supplemental 2). Taken together, these data imply that the inhibition observed results from the activation of approximately 50-100 presynaptic inputs. Given that the GABAergic neurons in the SNr are thought to be exclusively projection neurons[26], this is consistent with the finding that projection neuron collaterals form 79.4 ± 96.1 (s.d.) boutons per neuron within the SNr of the rat[13].

Assuming a modest or low probability of paired connections, our connectivity estimates imply that the extent of activation across a large population of SNr neurons would determine the extent of feedback inhibition consistent with our observation *in vivo*. While we do not have a direct measure of the total extent of activation of the SNr by our photostimulation, we note that neurons recorded simultaneously experience the same activation state of the network. Thus, we reasoned that the extent of feedback inhibition in a pair of recorded neurons should be correlated if feedback inhibition is proportional to the total activation of the network. Consistent with this prediction, we found that there was a significant correlation (Pearson's correlation, $p<0.01$ permutation test) in paired recordings (Figure 3i). These results suggest that a given SNr projection neuron receives input from a spatially diffuse collection of other SNr projection neurons.

The data above are consistent with the claim that a large population of SNr projection neurons must be recruited to fire within a relatively small time window (5-20 ms) in order to achieve robust feedback inhibition and divisive gain effects (Figure 3g). These results were obtained in the *Thy1*-ChR2 mouse where all neurons in the SNr express ChR2 (Figure 2). This would suggest that if a local subset of the SNr was expressing ChR2 the divisive gain effect should be present, but reduced in magnitude analogous to the smaller effects observed when less of the network was recruited in the *Thy1*-ChR2 preparation (Figure 3g). Indeed we found that when the same experiment was repeated in ChR2+ nigral neurons from virally infected *Gad2*-ChR2 mice a divisive gain effect was observed, but reduced in magnitude ($p<0.05$; two-factor ANOVA; 15% reduction in the saturated response).

Intrinsic properties that produce tonic spiking effectively counteract transient inhibition

To alter the gain of a response to activation of the network requires a change in the slope of the curve. As described above, we observed that there was a substantial effect of feedback inhibition in the strongly activated SNr circuit, but no effect in the absence of stimulation – resulting in a change in the slope of the response to stimulation. However, it is confusing how a strongly coupled inhibitory network of tonically active neurons could exhibit no effect of feedback even in the absence of stimulation. We first asked whether the rate of spontaneous IPSCs was consistent with our estimate, and a prior anatomical estimate[13], of >50 inputs from other SNr projection neurons. The expected rate of spontaneous IPSCs would thus be approximately:

$$R_{uIPSCs} = N_{pre} \times R_{pre} \times P_{release} \qquad (1)$$

Where R_{uIPSCs} is the predicted rate of unitary IPSCs (uIPSCs), N_{pre} is the number of presynaptic inputs (release sites), R_{pre} is the mean firing rate of presynaptic inputs, and $P_{release}$ is the effective release probability across all release sites. Thus, with a relatively low release probability (<0.5) we would predict 75-300 Hz of uIPSCs. This corresponds well to the rate of uIPSCs estimated directly from voltage clamp recordings (Figure 4a-c). Consistent with this estimate we also show that repetitive stimulation of SNr collaterals fails to completely depress transmission (Figure 4-

figure supplemental 2) consistent with a vesicular release probability low enough to allow vesicle recycling to keep pace with release. Such a mechanism has been described in detail for Purkinje cell synapses [27]. These observations suggest that there is indeed a substantial background rate of IPSCs that, when pharmacologically blocked, has no significant effect on the tonic firing of SNr projection neurons [28].

The question as we posed it - how can a strongly coupled inhibitory network of tonically active neurons exhibit no effect of feedback under basal conditions? - implies that tonic spiking is the problem. Alternatively, tonic spiking could be the solution. For a neuron to repetitively fire it must, upon the return from a spike, exhibit a net membrane current that is inward and thus drives the membrane towards spike threshold[29]. This implies a positive slope conductance combined with a net inward current below threshold[30] – in other words, the conductances that drive repetitive firing oppose hyperpolarizing currents in the perithreshold regime. Combined with a reduced driving force of inhibition near threshold, these biophysical features suggest that SNr neurons are much less sensitive to inhibition than to excitation in this regime. To test this hypothesis explicitly we performed dynamic clamp experiments in which we systematically varied the balance between a high background rate of IPSCs and EPSCs (Figure 4d-f). Indeed, we found that the sensitivity of the spike rate to increasing inhibition was much reduced compared to the sensitivity to increasing excitation. Stimulation strongly biased towards an inhibitory conductance often exhibited no effect on the mean spike rate relative to tonic levels. Consistent with the mechanistic model described above we found that the slope conductance in the perithreshold regime was indeed nonlinear with a sharp positive slope near the inhibitory reversal potential (Figure 4-figure supplemental 1). Moreover, we found that measured biophysical properties (*e.g.* slope conductance, spike threshold) were unaffected by pharmacological blockade of inhibition (Figure 4-figure supplemental 1).

The intrinsic inhibitory microcircuit provides a fast, transient inhibition

Collateral inhibition resulted in a strong suppression of evoked spiking and was sufficient to truncate evoked responses, often after only a few milliseconds. This suggested that collateral inhibition provided substantial inhibition that onset rapidly following stimulation. However, it is possible that the transient effect could also reflect properties of the photostimulation. To distinguish these possibilities we examined the kinetics of feedback inhibition and compared it to the main source of feed forward inhibition to the SNr from the striatum.

We made intracellular recordings from individual SNr projection neurons in *Gad2*-ChR2 mice to probe the properties of local feedback inhibition (Figure 5a-b) and from *Drd1a*-cre mice which were injected with a virus expressing a *cre*-dependent ChR2 transgene into the striatum to target the D1 receptor expressing medium spiny neurons which send axons directly into the SNr [31] (*Drd1a*-ChR2; Figure 5c). Postsynaptic neurons were recorded in the voltage clamp configuration with a holding potential of ~+20mV (reversal potential of the ChR2 current; Figure 2h-j) to isolate inhibitory postsynaptic currents (IPSCs). Slices were perfused with antagonists of excitatory synaptic transmission. Repeated pulses (10 Hz) of wide-field photostimulation elicited stimulus locked IPSCs in 15/23 SNr GABA neurons in the *Gad2*-ChR2 mouse line (Figure 5b) and 18/24 SNr GABA neurons in the *Drd1a*-ChR2 mouse (Figure 5c). Outward currents recorded following photostimulation of both inputs were completely abolished by application of Gbz (Figure 5b-c; $P<0.001$). Evoked IPSCs from feedback nigral collaterals recorded in *Gad2*-ChR2 mouse exhibited rapid kinetics characterized by short, monosynaptic latencies (Figure 5d: 1.93 ±

0.02 ms), rapid 10-90% rise times (Figure 5e; 0.53 ± 0.01 ms) and rapid decay time constants (τ) (Figure 5f; 5.64 ± 0.14 ms). In contrast to the intranigral inhibitory synapses, we found that striatonigral IPSCs recorded in *Drd1a*-ChR2 mouse had significantly longer latencies (Figure 5d; 2.51 ± 0.02 ms P<0.001), slower 10-90% rise times (Figure 5e; 0.75 ± 0.014 ms, P<0.001) and slower decay τ (Figure 5f; 9.00 ± 0.14 ms, P<0.001). Perhaps most surprisingly, we observed that with saturating stimulation, intranigral synapses contributed as large or greater inhibition than the major afferent source of inhibitory input, the direct pathway (Figure 5g).

To probe the short-term plasticity properties of feed forward (*Drd1a*-ChR2) and feedback (*Gad2*-ChR2) inhibition to the SNr we analyzed the amplitude of successive IPSCs. We found that collateral synapses within the SNr exhibited paired pulse ratios (PPR) less than 1 (Figure 5h; PPR = 0.91 ± 0.03). While, in direct contrast, the striatonigral synapse was modestly facilitating (Figure 5h; PPR = 1.17 ± 0.05). This latter observation was consistent with a previous study that used extracellular stimulation of the direct pathway [32]. The depressing nature of the PPR for local feedback inhibition is unlikely to reflect desensitization of ChR2 as repeated pulses were all suprathreshold under our stimulus conditions (Figure 2). These results are thus consistent with a rapid onset of feedback inhibition sufficient to truncate sustained activation of the SNr population.

We did not find any statistically significant differences between the kinetic properties seen between the IPSCs measured in slices from *Gad2*-ChR2 mice compared with those measured from *Thy1*-ChR2 mice (Figure 5-figure supplemental 1). This is consistent with both approaches selectively or predominantly activating SNr projection neurons. By contrast, the amplitude of IPSCs evoked by maximal stimulation was significantly reduced in slices taken from *Gad2*-ChR2 mice compared to those taken from *Thy1*-ChR2 mice (P<0.05; unpaired two-tailed t-test; Figure 5-figure supplemental 1). These differences presumably reflect the non-homogeneous expression of ChR2 in the virally infected SNr of *Gad2*-ChR2 mice.

Spatial organization of the local inhibitory microcircuit of the substantia nigra

Our results demonstrate a previously unappreciated potency of feedback inhibition in the SNr (Figure 5g). Collateral synapses provide sufficient inhibition to regulate the gain of the output of the basal ganglia even during strong activation of the network (Figure 3g). However, anatomical reconstruction of individual axons suggest a sparse connectivity within the SNr [13]. The modest amplitude of individual mIPSCs (~150 pS; Figure 3-figure supplemental 2) and the low cell density of the SNr[33] (~30,000 neurons in a ~4 mm^3 volume[34]) imply that feedback inhibition derives from a substantial volume. The maximal amplitude of evoked IPSCs was 10,000 pS. If we assume a <1% connection probability then we would predict that inhibition would be derived from neurons in a ~600 µm radius from a given postsynaptic neuron. Consistent with such a model our wide-field stimulation experiments suggested that feedback inhibition magnitude scaled similarly for pairs of neurons (Figure 3i). While reconstructions of individual axons have been studied in detail, such results cannot be used to reliably infer the convergence of input onto an individual projection neuron. Moreover, light-level anatomy data cannot reliably predict the functional impact of feedback inhibition. Thus, we next adapted the ChR2-assisited circuit mapping (CRACM) [35 36] method developed for the neocortex to study the interconnectivity within nigral microcircuit.

Using a 10X objective it was possible to contain the entire extent of the SN within a single field of view. We positioned either 81-point or 140-point grids of stimulation sites to cover the SN

(Figure 6a). To achieve high spatial resolution of ChR2 activation, we used a focused 470 nm laser beam that could be rapidly re-positioned to each point on the grid in a pseudorandom sequence that avoided nearest neighbors. The duration of the light pulse was gated so as to deliver brief (<1 ms) pulses of light at each stimulation site. To obtain reliable and spatially homogeneous expression of ChR2 across nigral projection neurons we used slices from the *Thy1*-ChR2 transgenic mouse line. Relative to wide-field stimulation or stimulation targeting axonal fibers we reduced the maximal power of the laser using neutral density filters and performed calibration experiments to find intensities that would evoke precise, time-locked spikes in a small number of neurons with somatodendritic arbors surrounding the stimulation site (Figure 6-figure supplemental 1). Our data were consistent with a requirement for propagating action potentials to elicit postsynaptic responses and we found no evidence in recorded neurons of direct axonal stimulation under these conditions (Figure 6-figure supplemental 1). Furthermore we focused on the rising phase and initial peak of IPSCs to bias our analysis towards transmission that resulted from highly reliable, low jitter spikes initiated at each stimulus site.

To measure the spatial organization of local inhibitory connectivity within the SNr, postsynaptic GABA neurons were clamped to V_h+20 mV in the presence of glutamate receptor antagonists. The peak amplitude of light-evoked IPSCs was determined for each stimulus position and response maps of IPSC amplitude as a function of stimulus position were generated (Figure 6a-c). While the viral-overexpression preparations do not provide homogeneous expression we found that the length scale of the intranigral microcircuit estimated using the *Gad2*-ChR2 mouse was consistent with that from the *Thy1*-ChR2 mouse (Figure 6c). To characterize the spatial organization of input to individual neurons we characterized the "receptive field" of feedback inhibition as the center of mass (COM) and the 25% isoinhibition contour (ISO; Figure 6d). Finally, the majority of the somatodendritic arbor of each neuron was reconstructed from image stacks acquired on a two-photon microscope (Figure 6d) that allowed us to estimate the COM of the dendritic arbor.

Feed forward and feedback inhibition have independent spatial organization

It has been proposed previously that collateral inhibition may be largely confined to topographic boundaries defined by feed forward input from the striatonigral pathway[13]. However, if feedback and feed forward input were organized in register, then feedback could not produce a signal proportional to the 'global' activation of the network. This would imply a collection of parallel channels each of which could exhibit strong feedback. By contrast, our recording data in vivo (Figure 1) suggested that feedback was proportional to the average activation across a large spatial extent of the SN. Thus, we next asked whether the feedback intranigral inhibition was organized in register with feed forward inhibition from the striatum.

If feedback inhibition were organized in register with feed forward inhibition, then we would predict that (1) the somatodendritic position of the postsynaptic neuron should predict the location of the inhibitory receptive field and (2) the spatial extent of inhibitory receptive fields should be matched to the topographic boundaries defined by feed forward inhibition. In contrast to the first prediction, we found that there was no correlation between the location of individual neurons and the source of the strongest inhibition within the SNr. In other words, we found that neurons with non-overlapping dendritic arbors could have largely overlapping inhibitory receptive fields (Figure 6d). We found no correlation between relative somatic

position and the correlation of the inhibitory receptive fields in neither coronal (*n* = 14) nor sagittal (*n* = 16) slices (Figure 6e-f).

To assess whether local inhibition in the SNr observed topographic boundaries defined by afferent inhibition we generated double transgenic mice in which ChR2 was expressed under control of the *Thy1* promoter and *cre*-recombinase was expressed under control of the D1 receptor (hereafter referred to as *Drd1a*-cre x *Thy1*-ChR2). We then made focal injections of a *cre*-dependent virus expressing a red fluorescent protein into the dorsal striatum 2-3 weeks prior to performing circuit mapping experiments in midbrain slices (Figure 7-figure supplemental 1). Clear axonal labeling could be readily observed in the SNr (Figure 7a; Figure 7-figure supplemental 1). The striatonigral projection exhibited the characteristic "dual nature" that has been observed following focal tracer injections in rats [33]. In each slice we performed circuit mapping for 3 to 6 projection neurons at a range of distances from the axonal termination fields (Figure 7a). We found that the correlation in the maps obtained from individual neurons was a monotonically decreasing function of distance between neurons (Figure 7b). However, we found no clear organization between the striatonigral projection and the maps of feedback inhibition (Figure 7a,c). The organization of the local inhibitory circuit in relation to the boundaries of striatonigral axonal tracing suggests that there could be a partial separation between the regions that receive input from the medial and lateral striatum (Figure 7d; Figure 7-figure supplemental 2). However, the consistent fall off of the correlation in inhibitory response maps across neurons (Figure 7b) suggests that projection neurons receive feedback inhibition from a diffuse microcircuit and independent of the discontinuous topography of feed forward input.

The spatiotemporal properties of Intranigral inhibition in vivo

The potency and diffuse organization of feedback inhibition suggested that collateral synapses from SNr projection neurons could be a powerful determinant of the activity of the SNr even in the presence of ongoing input from afferent sources. The *in vitro* preparation presumably reduces or eliminates structured activity in afferent sources of input that could either directly compete with or modulate the consequence of feedback inhibition. Moreover, the length constant of inhibition was similar in the sagittal and coronal planes (Figure 6e-f) and thus, the potency of inhibition measured *in vitro* is, if anything, an underestimate of the impact of intranigral inhibition. We next asked whether we could use a complementary approach to measure the extent of the intranigral microcircuit in the awake mouse. By contrast to the mapping experiments above where we measured at one location (neuron) and stimulated many other locations, we next used either a silicon probe electrode array (Figure 8a) or wire array (Figure 8-figure supplemental 1) with integrated optical fibers to stimulate at one (somewhat diffuse due to light scattering) location while measuring the spiking activity of SNr neurons at many neighboring locations.

Following implantation of a 64-site silicon probe array with integrated optical fiber into the SN of *Gad2*-ChR2 mice (Figure 8a), we observed single units with narrow waveforms and high baseline firing rates characteristic of SNr projection neurons (Figure 8b). The distribution of baseline firing rates obtained *in vivo* was closely matched to the same distribution obtained using on-cell recordings from identified SNr projection neurons *in vitro* (Figure 8c). We also confirmed that brief stimulation with a light pulse, like the stimulus used in the gain experiments in Figure 3, produced population responses similar in time course to those measured during response to natural stimuli (Figure 3-figure supplemental 1). We found that *in vivo*, as observed *in vitro*, stimulus pulses of increasing duration produced mixed responses in

the SNr population characterized by units with direct excitation and a subsequent delayed inhibition (Figure 8b, upper example) as well as units with a pure suppression of firing that onset with a short delay (~5 ms latency; Figure 8b, lower example).

A relatively constant level of inhibition combined with increasing excitatory drive can produce subtractive effects on the output spiking of a neuron. By contrast, divisive gain effects require that inhibition be recruited in proportion to changes in excitatory drive. Our *in vitro* data was consistent with a divisive gain effect on nigral output due to intranigral inhibition. To distinguish these two possibilities *in vivo* we examined neurons that exhibited apparent direct excitation (short-latency increase in stimulus evoked firing) with those that exhibited inhibition (stimulus evoked suppression of firing below baseline). We found that inhibition and excitation were recruited with a similar dependence on stimulus intensity consistent with a model in which intranigral inhibition produces a divisive gain effect on the output of SNr projection neurons (Figure 8d).

Finally, our circuit mapping data (Figure 6-7) suggested that functional inhibition extended for hundreds of microns within the SNr. To estimate the spatial extent of inhibition *in vivo* we next examined the position of excitatory and inhibitory responses on the electrode array. The location of each inhibitory and excitatory response is plotted as a function of position for the 20 ms and 50 ms stimulus conditions as a function of electrode position, maximal intensity projection, or cumulative histogram as a function of distance from the focus of excitation (Figure 8e). Taken together these data indicate that functional inhibition can extend for hundreds of microns beyond the focus of excitation *in vivo* as was observed *in vitro*.

DISCUSSION

The control of voluntary movement is well described by optimal feedback control models [37]. The basal ganglia is part of the extended brain circuit that controls voluntary movement [38]. Within this extended circuit there are a number of potential feedback projections [39]. However, the only intrinsic source of feedback to the main basal ganglia output nucleus, the SNr, is the microcircuit formed by collaterals of projection neurons [26]. Despite anatomical[26,40] and functional[41,42] evidence for the existence of this collateral microcircuit, its functional organization, relative impact, and properties were largely unknown. Here we show that the unique properties of the SNr microcircuit – both intrinsic properties of projection neurons and the organization of functional activity – combine to implement a potent feedback inhibitory circuit that can exert a divisive gain control effect on the basal ganglia output.

In behaving mice, we observed that the SN microcircuit appears to modify transient responses to salient sensory stimuli, in our case a CS, in a manner consistent with negative feedback (Figure 1). We subsequently used cell-type specific expression of ChR2 to show that (1) the inhibition provided by collaterals of SNr projection neurons was sufficient to dramatically suppress firing of projection neurons even in the presence of strong activation (Figure 3); (2) collateral synapses produced inhibition with a rapid onset and modest short-term depression allowing for sustained inhibition during repetitive firing (Figure 4-figure supplemental 2, Figure 5); (3) intranigral inhibition had distinct biophysical properties but comparable magnitude to the major source of feed forward input, the striatonigral pathway (Figure 5); (4) individual intranigral synapses were weak, but potent inhibition resulted from a spatially diffuse microcircuit *in vitro* (Figure 6-7) and *in vivo* (Figure 8). Together these data indicate that the functional architecture of the intranigral microcircuit is sufficient to provide robust feedback inhibition that is proportional to the activity SN population – *i.e.* it provides a potent gain control on the output of the basal ganglia.

Finally, existing anatomical studies were divided on whether the striatonigral and intranigral circuits were organized in spatial register [43 13]. The diffuse sources of collateral input to SNr projection neurons suggested that feedback inhibition extended across topographic divisions. We further confirmed this observation by combining axonal tracing together with circuit mapping to demonstrate that the striatonigral and intranigral projections were organized independently (Figure 7). Thus, our data imply that the gain control provided by the intranigral microcircuit could reflect a global negative feedback signal that spans individual channels of feed forward basal ganglia activity.

Optogenetic-based measurements of the intranigral microcircuit

In our experiments we used two approaches to achieve cell-type specific expression of ChR2 in the GABAergic projection neurons of the SNr. Both viral-mediated infection of GABAergic neurons in the SNr and the *Thy1*-ChR2 transgenic mouse line exhibited cell-type specific expression of ChR2 in GABAergic neurons of the SN, but not in dopamine neurons. GABAergic projection neurons and dopamine neurons are thought to be the only two cell types present in the rodent SN. Importantly, both approaches had indistinguishable properties of inhibition onto both GABAergic projection neurons (Figure 5-figure supplemental 1) and onto dopamine neurons[17]. Moreover, viral mediated expression allowed for the best possible quantitative comparison between feed forward and feedback pathways by ensuring that expression of the ChR2 was controlled by a common promoter (Figure 5). Thus, for these results the only

significant differences between the virally-mediated and transgenic expression of ChR2 in the SNr was the fraction of the population found to express ChR2 and the resultant magnitude of feedback inhibition. While viral-mediated expression could be used to estimate the divergence of inhibitory projections from a single stimulation site (Figure 8), it was not suitable for comprehensive mapping of convergence onto individual SNr neurons (Figures 6-7). The concern in a transgenic mouse line is that ChR2 expression could be present in afferent fibers. To control for this we blocked excitatory transmission, confirmed that light-activated currents had kinetics expected of ChR2 positive neurons, and confirmed that neurons of the major source of inhibitory input, the striatonigral pathway, did not express ChR2. Consistent with these observations it has previously been suggested that inhibitory fibers in this *Thy1*-ChR2 mouse line do not express ChR2[44]. However, in addition to expression in the SNr we did also observe that neurons of the external globus pallidus (GPe) express ChR2. The GPe is the source of a projection to the subthalamic nucleus and a more modest projection to the SNr [45 7]. Nonetheless, we found that potent feedback inhibition could be observed in *Gad2*-ChR2 mice and that stimulation of GPe axons yielded relatively less inhibition in SNr neurons than either the striatonigral or intranigral pathways under our stimulus conditions. Finally, we used laser powers that were attenuated relative to the powers necessary to directly stimulate severed axons in these mice [24], consistent with our observation that only perisomatic stimulation was sufficient to evoke reliable spiking in SNr neurons (Figure 6-figure supplemental 1).

A mechanism for divisive gain control in a circuit lacking interneurons

Unlike many other circuits in which gain control has been studied, projection neurons of the SNr are spontaneously active. Divisive gain control requires that there is little effect of inhibition in the absence of stimulation. In the case of gain control mediated by an interneuron this can be achieved in a number of ways, *e.g.*, through facilitating inhibitory synaptic transmission[46] (Figure 9). However, in spontaneously active neurons it is less clear how to prevent feedback inhibition from altering the baseline firing rate as we observe here. One possibility suggested by our data is that a broad distribution of firing rates (Figure 8) combined with relatively weak individual connections (Figure 4) could produce inhibition that is essentially tonic and too small to significantly affect intrinsic currents that drive repetitive spiking (Figure 4-figure supplemental 1) and so is counteracted via subthreshold inward currents necessary for repetitive firing. We provided support for such a model by demonstrating that there is, indeed, a high frequency (200 Hz) of spontaneous IPSCs bombarding SNr projection neurons (Figure 4). Further consistent with this model, simulation of a steady background rate of IPSCs using dynamic clamp revealed a relative insensitivity of spike rate to a tonic net inhibitory background of inputs (Figure 4). This balance in the tonic firing rate can be disrupted by synchronously recruiting neighboring neurons to produce a rapid inhibition that, combined with the positive feedback produced by inhibition and subsequent disinhibition, overcomes via de-activation[30] the inward currents that drive the membrane potential towards threshold. This mechanism combining intrinsic properties and synaptic properties is sufficient for a population of spontaneously active inhibitory neurons to implement divisive gain control in the apparent absence of interneurons[26]. To our knowledge this represents a novel circuit mechanism for divisive gain control[47] (Figure 9).

The multiple roles of intranigral inhibition: feedback vs. lateral inhibition

One can think of two possible regimes in which the SNr may operate and each has distinct implications for the function and role of intranigral inhibition. On the one hand, it has been argued for some time that the feed forward pathways of the basal ganglia are topographically organized and largely independent [4,9,6]. Movement is thus thought to occur when a focal

population of projection neurons becomes inhibited by feed forward input and thus disinhibits downstream pre-motor structures. From this perspective, the diffuse intranigral microcircuit could act to release neighboring projection neurons from intranigral inhibition and thereby suppress unintended movements. Thus, during focal activation of the SNr, collateral inhibition may be thought of as a mechanism for contrast enhancement akin to the role of lateral inhibition in sensory systems. This mechanism may be reflected in the time locked, bidirectional changes in the firing of SNr projection neurons that are commonly observed prior to and during movement in mice[48,49] and primates[50,51].

On the other hand, while the direct striatonigral pathway is topographically organized there is considerable divergence in the corticostriatal input in mice[52]. In addition, there may be less precise topographic organization of the indirect pathway that enters the SNr via the subthalamic nucleus [53]. The subthalamic nucleus also receives direct cortical input and ascending input from the midbrain [54] and hindbrain [55,56]. The topographic organization of these ascending pathways is less well understood. Regardless of the topographic precision, the inputs that arrive at the SNr from the subthalamic nucleus convey a great diversity of information and likely exhibit a diversity of dynamics. While there are mechanisms that could maintain activity within a fixed dynamic range in upstream structures[46], individual neurons that constitute the output of cortical areas project to multiple subcortical structures[57]. It is therefore unlikely that the dynamic range of even the cortical output is appropriate for the diverse computations performed in all target structures. To effectively control the basal ganglia output in the presence of such diverse input dynamics and anatomical divergence would seem to require coordinated processing across functional domains. Thus, divisive gain control supplied by a diffuse but potent inhibitory microcircuit could be well suited to ensure that activity remains within a fixed dynamic range.

We favor a model in which these contrasting descriptions of the role of the intranigral microcircuit are two aspects of its function that can be engaged in different input regimes. The diffuse organization that could produce lateral inhibition in some regimes under the animal's control (*i.e.*, activation of specific well learnt actions), but, may be necessary to produce divisive gain control in other regimes (*i.e.*, 'global' activation of the SNr by salient stimuli). While it is not currently possible to monitor nigral dynamics during selective manipulation of feedback, but not feed forward or efferent inhibition, such an approach will be required to definitively test the predictions of our work.

The impact of intranigral inhibition on the function of the basal ganglia

Simple geometrical considerations suggest that the intranigral microcircuit integrates functionally distinct information on a large scale. Cortical afferents to the basal ganglia are derived from an estimated 17 million neurons[58] spanning the majority of the roughly 100 mm^3 volume of neocortex. These inputs are funneled through the basal ganglia and will ultimately terminate on approximately 30,000 projection neurons[34] within the roughly 4 mm^3 volume of the SN. Dendrites of nigral projection neurons and intranigral inhibition that extends over hundreds of microns [43,59] could therefore shape activity derived from cortical inputs separated by several millimeters.

Existing functional models focus on the feed forward structure of processing within the intrinsic basal ganglia circuitry (*e.g.*, [60,1,4]). However, our observation that intranigral inhibition is strong relative to the major source of feed forward input suggests that local processing of diverse streams of information in the SN could be critical for generating dynamics in the basal ganglia

output. We hypothesize that the diverse impairments characteristic of pathological disruption of basal ganglia function could reflect, in part, a control system operating outside of a stable regime. Although there is evidence of perturbed dynamics in the SNr in disease models[61-63], the specific contribution of the intranigral microcircuit to the diverse behavioral impairments observed in diseases afflicting the basal ganglia circuit remains unclear.

ACKNOWLEDGEMENTS

Susan Jones, Vivek Jayaraman, Alla Karpova, Albert Lee, Jeff Magee, Gabe Murphy and Nelson Spruston provided critical feedback at various stages of preparation of the manuscript and progression of the project. We are indebted to the extensive feedback from our colleagues following presentation of this work at internal seminars on the Janelia Farm Research Campus.

JB and JTD designed the experiments. JTD and JB analyzed the data. JTD, JB, and WXP wrote the manuscript. JB and WXP performed the *in vivo* recording experiments. JB performed the *in vitro* experiments. We thank members of the lab for critical reading and feedback on the manuscript. JB is a graduate scholar in the Cambridge-Janelia Farm Graduate Program. JTD is a JFRC Fellow of the Howard Hughes Medical Institute. This work was supported by funding from the Howard Hughes Medical Institute. The authors declare no competing financial interests. Correspondence and requests for materials should be addressed to dudmanj@janelia.hhmi.org.

MATERIALS AND METHODS

Animals

For *in vitro* experiments, adult transgenic mice (10-30 weeks old) expressing either; ChR2-YFP fusion gene under the control of the mouse thymus cell antigen 1 promoter (Line 18, Stock #007612, Jackson Labs, '*Thy1*' mice), *cre*-recombinase under the control of the glutamic acid decarboxylase 2 gene (Stock #010802, Jackson Labs, 'GADcre' mice) or *cre*-recombinase under the control of the dopamine receptor D1A (GENSAT[64], Rockefeller University, '*Drd1a*-cre' mice). For *in vivo* electrophysiology experiments, four adult (30 g, 3-6 months old) *Thy1* mice were used. All animals were handled in accordance with guidelines approved by the Institutional Animal Care and Use Committee of Janelia Farm Research Campus. The experimenter was not blinded to genotype.

Animal care

Mice were housed in a temperature- and humidity- controlled room maintained on a reversed 12 h light/dark cycle. For *in vivo* physiology experiments, mice were housed individually. For *in vitro* experiments, mice were group housed (1-5 mice per cage).

Viral expression

We used 3 adeno-associated viruses (AAV, serotype 2/1) to achieve either conditional expression of ChR2 and tdTomato or pan-neuronal expression of eGFP and tdTomato. Viruses were produced at the Molecular Biology Shared resource of Janelia Farm Research Campus. Where indicated similar viruses can be obtained publicly from the Gene Therapy Program at the University of Pennsylvania (http://www.med.upenn.edu/gtp/vectorcore/Catalogue.shtml). Conditional ChR2 expression was achieved with AAV2/1 SYN-FLEX-ChR2-GFP *analogous to* AV-1-18917P. Conditional tdTomato expression was achieved with AAV2/1 CAG-FLEX-tdTomato-WPRE-bGH *available as* AV-1-ALL864. Pan-neuronal expression of tdTomato and eGFP were obtained via AAV2/1 SYN-[tdTomato/eGFP]-WPRE-SV40 *available as* AV-1-PV1696.

Viruses were injected into the striatum (STR) of *Drd1a*-cre mice, globus pallidus (GP) or substantia nigra (SN) of GADcre mice, in a fashion similar to that previously described [22]. Briefly, under deep anesthesia, a small craniotomy was made over the STR (0.5 mm anterior-posterior, 1-2 mm medial-lateral, -2.5 mm dorso-ventral), GP (-0.45 mm anterior-posterior, -1.8 mm medial-lateral, -3.6 mm dorsal-ventral) or SN (-3 mm anterior-posterior, 1 mm medial-lateral, -4.2 mm dorso-ventral). A glass pipette was used to pressure inject small volumes of virus (20-100 nL per injection site). Animals were allowed to recover for at least 2 weeks following surgery.

In vitro electrophysiology

Briefly, adult mice were deeply anaesthetized under isoflurane, decapitated and the brains were dissected out into ice-cold modified artificial cerebral spinal fluid (aCSF) (52.5 mM NaCl, 100 mM sucrose, 26 mM $NaHCO_3$, 25 mM glucose, 2.5 mM KCl, 1.25 mM NaH_2PO_4, 1 mM $CaCl_2$, 5 mM $MgCl_2$ and 100 µM kynurenic acid) that had been saturated with 95% O_2/5% CO_2. 300 µM thick coronal and sagittal slices (as indicated in the text) were cut (Leica VT1200S; Leica Microsystems, Germany), transferred to a holding chamber and incubated at 35°C for 30 minutes in modified aCSF (119 mM NaCl, 25 mM $NaHCO_3$, 28 mM glucose, 2.5 mM KCl, 1.25 mM NaH_2PO_4, 1.4 mM $CaCl_2$, 1 mM $MgCl_2$, 3 mM sodium pyruvate, 400 µM ascorbate and 100 µM kynurenic acid, saturated with 95 % O_2/5% CO_2) and then stored at 21°C.

For recordings, slices were transferred to a recordings chamber perfused with modified aCSF (119 mM NaCl, 25 mM $NaHCO_3$, 11 mM glucose, 2.5 mM KCl, 1.25 mM NaH_2PO_4, 1.4 mM $CaCl_2$, 1 mM $MgCl_2$, 3 mM sodium pyruvate, 400 µM ascorbate, saturated with 95% O_2/5% CO_2) and maintained at 32-34°C at a flow rate of 2-3 ml min^{-1}. For mIPSC experiments, extracellular Ca^{2+} was replaced with 2 mM Sr^{2+} to desynchronize release. Patch pipettes (resistance = 5-8 MΩ) were pulled on a laser micropipette puller (Model P-2000, Sutter Instrument) and filled with one of the following intracellular solutions: Current-

clamp recordings of spike activity used a potassium gluconate-based intracellular solution (137.5 mM potassium gluconate, 2.5 mM KCl, 10 mM HEPES, 4 mM NaCl, 0.3 mM GTP, 4 mM ATP, 10 mM phosphocreatine, pH 7.5). Voltage-clamp recordings for IPSC measurements used a $CeMeSO_4$-based intracellular solution (114 mM $CeMeSO_4$, 4 mM NaCl, 10 mM HEPES, 5 mM QX314.Cl, 0.3 mM GTP, 4 mM ATP, 10 mM phosphocreatine, pH 7.5). Alexa Fluor 488 or Alexa Fluor 568 was commonly added to intracellular solution to aid cell visualization and *post hoc* reconstruction. In some experiments the following were added as indicated in the text: 10 µM CNQX or 5 µM NBQX, 50 µM D-AP5, 10 µM gabazine (Gbz), 0.5 µM tetrodotoxin (TTX). All drugs were obtained from Tocris Biosciences. Intracellular recordings were made using a MultiClamp700B amplifier (Molecular Devices) interfaced to a computer using an analog to digital converter (PCI-6259; National Instruments) controlled by custom written scripts (to be made available at http://dudmanlab.org/) in Igor Pro (Wavemetrics). Photostimulation was carried out using a dual scan head raster scanning confocal microscope and control software developed by Prairie Systems, and incorporated into a BX51 upright microscope (Olympus America).

Individual neurons were patched under DIC optics with a water-immersion 40X objective. Spiking was measured in the cell-attached configuration. The spiking frequency and action potential waveform were used to classify neurons as DA or GABA as described previously[17]. Upon break in while diffusion of QX314 was allowed time to progress, negative voltage clamp steps were used to measure the hyperpolarization-activated inward (Ih) current. The presence of detectable inward currents was diagnostic for DA neurons. In current clamp recordings lacking QX314 in the internal solution the intracellular spike waveform and spontaneous firing frequency were further used to confirm cell identity. Analysis of postsynaptic currents (direct photocurrents, sIPSC, mIPSCs and evoke IPSCs) and spiking was performed using custom written analysis code in Igor Pro (Wavemetrics). Peak current amplitude was measured as the peak synaptic current relative to the baseline holding current preceding each stimulus. Tonic current amplitude was measured as the peak evoked synaptic current relative to the holding current preceding each train. The conductance (g) underlying IPSCs were calculated from $g = IPSC_{peak}/(V_m\text{-}EGABA_A)$, where $IPSC_{peak}$ is the peak amplitude of the IPSC and V_m is the holding voltage. The equilibrium potential of $GABA_A$ current (EGABA) was estimated at -70 mV from the Nernst equation. Rise time constants of postsynaptic currents were measured by finding the 20-80% slope of the rising phase of the stimulus-evoked current. Decay time constant of postsynaptic currents were measured by fitting a single exponential to the decay phase of the stimulus-evoked currents.

Spikes were detected at the threshold of maximum acceleration. Phase plots were constructed by plotting the first derivative of the somatic membrane potential (dV/dt) versus the somatic membrane potential for the average spike waveform. The membrane potential at which phase plot slope reached 10 $mV \cdot ms^{-1}$ was denoted the voltage threshold and a linear fit was used to calculate the slope. The perithreshold slope was calculated as the slope of the 'kink' defined as the slope of dV/dt for 7 ms after the peak of the perithreshold dV/dt.

For dynamic clamp experiments, individual postsynaptic conductances were generated using IGOR Pro (Wavemetrics), from the sum of two exponentials with rise tau and decay tau derived from measured IPSC and EPSC rise and decay kinetics (rise tau = 0.5 ms, decay tau = 5 ms). The times of individual events were computed by sampling a Poisson distribution in which the rate of IPSC and EPSC events were independently changed from 1000 to 5000 Hz to generate different balances of excitation and inhibition. The convolved waveforms for excitation and inhibition were computed independently and passed to a custom made, digital dynamic clamp (update rate 30 kHz; to be described elsewhere) assuming reversal potentials of -70 mV and 0 mV for inhibition and excitation, respectively.

Optical stimulation and imaging

The optics were designed to minimize the spread of the laser in the x,y dimensions of the focal plane while accentuating the focus in z by underfilling the back aperture of the objective. Stimulation intensity was controlled by pulse duration (0.2-1 ms). Stimulation typically consisted of 9x9 and 10x14 maps of stimulation sites with independent stimuli being delivered in a pseudo-random (non-neighbor) sequence

at an interstimulus interval of ≥150 ms) and values reflect the average of 3-4 repetitions of the mapping experiment for each cell. Stimulation strength was modulated by gating the laser at maximal power (473 nm, AixiZ or 488 nm, BlueSky Research) with varying durations using timing signals from an external pulse controller (PrairieView software) and the internal power modulation circuitry of the laser or an external Pockels cell (Conoptics) with indistinguishable results. Wide-field activation of ChR2 was accomplished using blue LED (470 nm, ThorLabs) transmitted through the fluorescence light path of the BX51 microscope. LED intensity and timing were controlled through a variable current source (ThorLabs). Stimulus families (input/output curves) were delivered in a pseudorandom order and repeated 3-10 times per cell.

Analysis of mapping data

Analysis was performed using custom written routines for Igor Pro (Wavemetrics) and Matlab R2011a (Math Works). Analysis of the full field photostimulation was performed using standard analysis metrics as described in the text. To attempt to minimize the variability in estimates of short-term plasticity stimulation was performed at the half-maximum stimulus intensity determined by generation of an input-output function at the beginning of the experiment. The analysis of circuit mapping experiments was more complicated and is described briefly below and demonstrated more explicitly in Figure 6. Briefly, averages of 3 to 10 multisite photostimulation experiments were used in all analyses. The moment of photostimulation was determined by thresholding a photodiode signal positioned in a parallel light path to the stimulation light path. Galvonometer position signals were recovered from the PrairieView software and aligned using a transmitted light laser scanning DIC image of the brain slice. Offline analysis routines automatically detected the orientation of the stimulus grid and applied a rotation to put that grid into 0 rotation orientation. The dorsal and medial edges of the grid were manually annotated and used to flip or further rotate all grids into a common reference frame. The average dimensions of the SN are 1.67 mm wide by 1 mm tall. We found that the average of all grids had an identical (1.67 to 1) aspect ratio. There was modest variation (~10%) in the dimensions of the SNr grids. All grids were linearly stretched or compacted to the same mean aspect ratio and cell positions moved accordingly. Qualitatively similar results were obtained in the presence and absence of warping. Full depth maps were generated by convolving the response amplitude at individual stimulus positions with an empirically-estimated Gaussian response function. An isocontour of the resulting image was generated at the half maximum level using the 'contour' function supplied by Matlab. The center of mass (COM) was also calculated as the vector average of the Euclidean distance to the stimulus position weighted by response magnitude.

Reconstructions of recorded neurons were derived from two-photon fluorescent image stacks using the semi-automated software generously provided by Ting Zhao (Janelia Farm Research Campus, HHMI)[65]. The COM of the dendrites was calculated as the vector average with the weights defined by the width of the dendritic branch segment at the end of the vector position. Data was then loaded into Matlab for display and scaling.

In vivo electrophysiology

Recordings were performed using either a 32-microwire arrays (CD Neural Technologies) or a 64-channel silicon probe array (NeuroNexus Technologies). Electrode arrays were stereotaxically implanted under anesthesia (isoflurane; 1.5-2.5% in O_2) in mice that had been previously fitted with a plastic head restraint and held in place by a custom head fixation system[66]. Design files and details about the manufacture and use of our head restraint system are available online (http://dudmanlab.org/html/rivets.html). Electrode arrays were targeted to the SN of the ventral midbrain (3.0-4.5 mm posterior to bregma, 0.5-2.0 mm lateral to midline and >3.5 mm below the surface of skull). Electrode arrays were maintained in position by a micromanipulator (Sutter Instruments or Scientifica) and connected to the recording systems via a flexible wire coupling and connector. For optogenetic experiments, a 200 μm core multimode fiber (ThorLabs) was affixed near the central recording wires of a 32 channel array or to one shank of the silicon probe array as indicated in Figure 8a. The entire array was slowly lowered in to the midbrain. Following >1 hour of recovery single unit recordings were obtained from alert, but quietly resting mice. Single cell isolation was performed offline using Offline Sorter (Plexon Technologies) and standard techniques.

Analysis of stimulus-evoked responses were calculated and presented using Matlab 2011a.

The spike data in Figure 1 are a subset of recording sessions (all sessions with ≥8 simultaneously recorded, putative GABAergic cells) from mice performing an auditory trace conditioning task described in detail previously [17]. Briefly, mice were trained to consume sweetened water rewards delivered from a port placed on one wall of a behavior box. A speaker placed behind one wall of the box delivered pure tones (10 kHz; 500 ms duration) as conditioned stimuli (CS). Water rewards were delivered 2.5 sec following CS onset. This dataset included 599 single units recorded across sessions in which 5 to 21 units were recorded simultaneously. For each session we computed the firing rate of the population of units prior to the onset of the CS and the transient response in the 200 ms following CS onset and subtracted the mean response across all trials. For each trial and all units recorded in a given session we then computed the population response excepting the ith unit ($PRE_{population}$) and the response of the ith unit to the CS ($RESP_{single}$). For individual sessions we determined the correlation between $PRE_{population}$ and $RESP_{single}$ for all units in the session. Significance of the correlation was determined using a permutation test. For the entire population we plotted $PRE_{population}$ vs. $RESP_{single}$ for all units, all trials. The data was binned into 20 equally spaced bins and mean data for all bins with more than 5 samples was plotted and fit with a sigmoid function using Igor Pro.

Statistics

All statistical tests were performed using the statistics package from Matlab 2011a (Math Works). Paired comparisons were performed using the student's t-test (all results were also confirmed with a non-parametric ranksum test). Multiple comparisons were performed using ANOVA. Significance was defined as $p<0.05$ unless otherwise indicated. Averaged data are presented as mean ± standard error of the mean (SEM), unless otherwise specified.

REFERENCES

1 DeLong, M. R. in *Principles in Neural Science* (ed E.R. and Scwartz Kandel, J. and Jessell, T.M.) Ch. 43, 853-872 (McGraw Hill, 2000).

2 Buhusi, C. V. & Meck, W. H. What makes us tick? Functional and neural mechanisms of interval timing. *Nat Rev Neurosci* **6**, 755-765 (2005).

3 Turner, R. S. & Desmurget, M. Basal ganglia contributions to motor control: a vigorous tutor. *Curr Opin Neurobiol* **20**, 704-716, doi:10.1016/j.conb.2010.08.022 (2010).

4 Mink, J. W. The basal ganglia: Focused selection and inhibition of competing motor programs. *Progress in Neurobiology* **50**, 381-425 (1996).

5 Diedrichsen, J., Shadmehr, R. & Ivry, R. B. The coordination of movement: optimal feedback control and beyond. *Trends in cognitive sciences* **14**, 31-39, doi:10.1016/j.tics.2009.11.004 (2010).

6 Haber, S. N. The primate basal ganglia: parallel and integrative networks. *J Chem Neuroanat* **26**, 317-330 (2003).

7 Gerfen, C. R. in *The Rat Nervous System* (ed G. Paxinos) Ch. 18, 458-497 (Elsevier, 2004).

8 Astrom, K. J. a. M., R.M. *Feedback Systems*. (Princeton University Press, 2008).

9 Hikosaka, O. GABAergic output of the basal ganglia. *Progress in Brain Research* **160**, 209-226 (2007).

10 Parent, A. Extrinsic connections of the basal ganglia. *Trends in Neurosciences* **13**, 254-258 (1990).

11 Cebrián, C., Parent, A. & Prensa, L. Patterns of axonal branching of neurons of the substantia nigra pars reticulata and pars lateralis in the rat. *The Journal of Comparative Neurology* **492**, 349-369 (2005).

12 Deniau, J. M., Mailly, P., Maurice, N. & Charpier, S. in *Gaba and the Basal Ganglia - From Molecules to Systems* Vol. Volume 160 (eds Elizabeth D. Abercrombie James M. Tepper & J. Paul Bolam) 151-172 (Elsevier, 2007).

13 Mailly, P., Charpier, S., Menetrey, A. & Deniau, J.-M. Three-dimensional organization of the recurrent axon collateral network of the substantia nigra pars reticulata neurons in the rat. *The Journal of Neuroscience: The Official Journal of the Society for Neuroscience* **23**, 5247-5257 (2003).

14 Tepper, J. M. & Lee, C. R. GABAergic control of substantia nigra dopaminergic neurons. *Progress in Brain Research* **160**, 189-208 (2007).

15 Brazhnik, E., Shah, F. & Tepper, J. M. GABAergic afferents activate both GABAA and GABAB receptors in mouse substantia nigra dopaminergic neurons in vivo. *The Journal of Neuroscience: The Official Journal of the Society for Neuroscience* **28**, 10386-10398 (2008).

16 Schmidt, R., Leventhal, D. K., Mallet, N., Chen, F. & Berke, J. D. Canceling actions involves a race between basal ganglia pathways. *Nature neuroscience* **16**, 1118-1124, doi:10.1038/nn.3456 (2013).

17 Pan, W. X., Brown, J. & Dudman, J. T. Neural signals of extinction in the inhibitory microcircuit of the ventral midbrain. *Nature neuroscience* **16**, 71-78, doi:10.1038/nn.3283 (2013).

18 Hammond, C., Shibazaki, T. & Rouzaire-Dubois, B. Branched output neurons of the rat subthalamic nucleus: Electrophysiological study of the synaptic effects on identified cells in the two main target nuclei, the entopeduncular nucleus and the substantia nigra. *Neuroscience* **9**, 511-520 (1983).

19 Zhang, F., Wang, L. P., Boyden, E. S. & Deisseroth, K. Channelrhodopsin-2 and optical control of excitable cells. *Nature methods* **3**, 785-792, doi:10.1038/nmeth936 (2006).

20 Boyden, E. S., Zhang, F., Bamberg, E., Nagel, G. & Deisseroth, K. Millisecond-timescale, genetically targeted optical control of neural activity. *Nature neuroscience* **8**, 1263-1268, doi:10.1038/nn1525 (2005).

21 Nevet, A., Morris, G., Saban, G., Arkadir, D. & Bergman, H. Lack of spike-count and spike-time correlations in the substantia nigra reticulata despite overlap of neural responses. *Journal of neurophysiology* **98**, 2232-2243 (2007).

22 Atasoy, D., Aponte, Y., Su, H. H. & Sternson, S. M. A FLEX switch targets Channelrhodopsin-2 to multiple cell types for imaging and long-range circuit mapping. *J Neurosci* **28**, 7025-7030 (2008).
23 Arenkiel, B. R. *et al.* In vivo light-induced activation of neural circuitry in transgenic mice expressing channelrhodopsin-2. *Neuron* **54**, 205-218 (2007).
24 Azdad, K. & Dudman, J. T. *submitted*.
25 Schmidt, R., Leventhal, D. K., Mallet, N., Chen, F. & Berke, J. D. Canceling actions involves a race between basal ganglia pathways. *Nat Neurosci*, doi:10.1038/nn.3456 (2013).
26 Deniau, J. M., Mailly, P., Maurice, N. & Charpier, S. The pars reticulata of the substantia nigra: a window to basal ganglia output. *Prog Brain Res* **160**, 151-172 (2007).
27 Telgkamp, P., Padgett, D. E., Ledoux, V. A., Woolley, C. S. & Raman, I. M. Maintenance of high-frequency transmission at purkinje to cerebellar nuclear synapses by spillover from boutons with multiple release sites. *Neuron* **41**, 113-126 (2004).
28 Atherton, J. F. & Bevan, M. D. Ionic mechanisms underlying autonomous action potential generation in the somata and dendrites of GABAergic substantia nigra pars reticulata neurons in vitro. *The Journal of Neuroscience: The Official Journal of the Society for Neuroscience* **25**, 8272-8281 (2005).
29 Raman, I. M. & Bean, B. P. Ionic currents underlying spontaneous action potentials in isolated cerebellar Purkinje neurons. *The Journal of neuroscience : the official journal of the Society for Neuroscience* **19**, 1663-1674 (1999).
30 Nolan, M. F. *et al.* The hyperpolarization-activated HCN1 channel is important for motor learning and neuronal integration by cerebellar Purkinje cells. *Cell* **115**, 551-564 (2003).
31 Gerfen, C. R. Synaptic organization of the striatum. *J Electron Microsc Tech* **10**, 265-281 (1988).
32 Connelly, W. M., Schulz, J. M., Lees, G. & Reynolds, J. N. J. Differential Short-Term Plasticity at Convergent Inhibitory Synapses to the Substantia Nigra Pars Reticulata. *J. Neurosci.* **30**, 14854-14861 (2010).
33 Gerfen, C. R. in *The Rat Nervous System* (ed G. Paxinos) Ch. 18, 458-497 (Elsevier, 2004).
34 Oorschot, D. E. Total number of neurons in the neostriatal, pallidal, subthalamic, and substantia nigral nuclei of the rat basal ganglia: a stereological study using the cavalieri and optical disector methods. *The Journal of Comparative Neurology* **366**, 580-599 (1996).
35 Wang, H. *et al.* High-speed mapping of synaptic connectivity using photostimulation in Channelrhodopsin-2 transgenic mice. *Proceedings of the National Academy of Sciences of the United States of America* **104**, 8143-8148, doi:10.1073/pnas.0700384104 (2007).
36 Petreanu, L., Huber, D., Sobczyk, A. & Svoboda, K. Channelrhodopsin-2-assisted circuit mapping of long-range callosal projections. *Nature neuroscience* **10**, 663-668, doi:10.1038/nn1891 (2007).
37 Wolpert, D. M. & Ghahramani, Z. Computational principles of movement neuroscience. *Nature neuroscience* **3 Suppl**, 1212-1217 (2000).
38 Kandel, E. R., Schwartz, J. H. & Jessell, T. M. *Principles of neural science*. 4th edn, (McGraw-Hill, Health Professions Division, 2000).
39 Dudman, J. T. & Gerfen, C. R. in *The Rat Nervous System* (ed G Paxinos) (Elsevier, 2014).
40 Mailly, P., Charpier, S., Menetrey, A. & Deniau, J. M. Three-dimensional organization of the recurrent axon collateral network of the substantia nigra pars reticulata neurons in the rat. *The Journal of neuroscience : the official journal of the Society for Neuroscience* **23**, 5247-5257 (2003).
41 Tepper, J. M., Abercrombie, E. D. & Bolam, J. P. in *Progress in Brain Research* Vol. 1 339 (Elsevier, 2007).
42 Tepper, J. M., Martin, L. P. & Anderson, D. R. GABAA receptor-mediated inhibition of rat substantia nigra dopaminergic neurons by pars reticulata projection neurons. *The Journal of Neuroscience: The Official Journal of the Society for Neuroscience* **15**, 3092-3103 (1995).
43 Grofova, I., Deniau, J. M. & Kitai, S. T. Morphology of the substantia nigra pars reticulata projection neurons intracellularly labeled with HRP. *The Journal of Comparative Neurology* **208**, 352-368 (1982).
44 Gradinaru, V., Mogri, M., Thompson, K. R., Henderson, J. M. & Deisseroth, K. Optical deconstruction of parkinsonian neural circuitry. *Science* **324**, 354-359, doi:10.1126/science.1167093 (2009).

45 Bolam, J. P., Hanley, J. J., Booth, P. A. C. & Bevan, M. D. Synaptic organisation of the basal ganglia. *Journal of Anatomy* **196**, 527-542 (2000).
46 Silver, R. A. Neuronal arithmetic. *Nat Rev Neurosci* **11**, 474-489, doi:10.1038/nrn2864 (2010).
47 Silver, R. A. in *Nat Rev Neurosci* Vol. 11 474-489 (2010).
48 Pan, W. X. a. B., J. and Dudman, J.T. Neural signals of extinction in the inhibitory microcircuit of the ventral midbrain. *Nature Neuroscience* (in press).
49 Fan, D., Rossi, M. A. & Yin, H. H. Mechanisms of action selection and timing in substantia nigra neurons. *J Neurosci* **32**, 5534-5548 (2012).
50 Turner, R. S. & Anderson, M. E. Pallidal discharge related to the kinematics of reaching movements in two dimensions. *J Neurophysiol* **77**, 1051-1074 (1997).
51 Nevet, A., Morris, G., Saban, G., Arkadir, D. & Bergman, H. Lack of spike-count and spike-time correlations in the substantia nigra reticulata despite overlap of neural responses. *J Neurophysiol* **98**, 2232-2243, doi:10.1152/jn.00190.2007 (2007).
52 Pan, W. X., Mao, T. & Dudman, J. T. Inputs to the dorsal striatum of the mouse reflect the parallel circuit architecture of the forebrain. *Frontiers in neuroanatomy* **4**, 147, doi:10.3389/fnana.2010.00147 (2010).
53 Bolam, J. P., Hanley, J. J., Booth, P. A. & Bevan, M. D. Synaptic organisation of the basal ganglia. *J Anat* **196 (Pt 4)**, 527-542 (2000).
54 Coizet, V. *et al.* Short-latency visual input to the subthalamic nucleus is provided by the midbrain superior colliculus. *The Journal of neuroscience : the official journal of the Society for Neuroscience* **29**, 5701-5709 (2009).
55 Winn, P. How best to consider the structure and function of the pedunculopontine tegmental nucleus: evidence from animal studies. *Journal of the neurological sciences* **248**, 234-250, doi:10.1016/j.jns.2006.05.036 (2006).
56 Bevan, M. D. & Bolam, J. P. Cholinergic, GABAergic, and glutamate-enriched inputs from the mesopontine tegmentum to the subthalamic nucleus in the rat. *The Journal of neuroscience : the official journal of the Society for Neuroscience* **15**, 7105-7120 (1995).
57 Kita, T. & Kita, H. The subthalamic nucleus is one of multiple innervation sites for long-range corticofugal axons: a single-axon tracing study in the rat. *The Journal of neuroscience : the official journal of the Society for Neuroscience* **32**, 5990-5999, doi:10.1523/JNEUROSCI.5717-11.2012 (2012).
58 Zheng, T. & Wilson, C. J. Corticostriatal combinatorics: the implications of corticostriatal axonal arborizations. *Journal of neurophysiology* **87**, 1007-1017 (2002).
59 Mailly, P. *et al.* Dendritic arborizations of the rat substantia nigra pars reticulata neurons: spatial organization and relation to the lamellar compartmentation of striato-nigral projections. *The Journal of Neuroscience: The Official Journal of the Society for Neuroscience* **21**, 6874-6888 (2001).
60 Albin, R. L., Young, A. B. & Penney, J. B. The functional anatomy of basal ganglia disorders. *Trends in Neurosciences* **12**, 366-375 (1989).
61 Ibanez-Sandoval, O. *et al.* Bursting in substantia nigra pars reticulata neurons in vitro: possible relevance for Parkinson disease. *Journal of neurophysiology* **98**, 2311-2323, doi:10.1152/jn.00620.2007 (2007).
62 Samadi, P. *et al.* Normalization of GABAA receptor specific binding in the substantia nigra reticulata and the prevention of L-dopa-induced dyskinesias in MPTP parkinsonian monkeys. *Synapse* **62**, 101-109, doi:10.1002/syn.20469 (2008).
63 Wang, Y. *et al.* Changes in firing rate and pattern of GABAergic neurons in subregions of the substantia nigra pars reticulata in rat models of Parkinson's disease. *Brain Res* **1324**, 54-63, doi:10.1016/j.brainres.2010.02.008 (2010).
64 Gong, S., Kus, L. & Heintz, N. Rapid bacterial artificial chromosome modification for large-scale mouse transgenesis. *Nature protocols* **5**, 1678-1696, doi:10.1038/nprot.2010.131 (2010).
65 Zhao, T. *et al.* Automated reconstruction of neuronal morphology based on local geometrical and global structural models. *Neuroinformatics* **9**, 247-261, doi:10.1007/s12021-011-9120-3 (2011).

66 Osborne, J. E. & Dudman, J. T. RIVETS: a mechanical system for in vivo and in vitro electrophysiology and imaging. *PloS one* **9**, e89007, doi:10.1371/journal.pone.0089007 (2014).

67 Deniau, J. M., Hammond, C., Riszk, A. & Feger, J. Electrophysiological properties of identified output neurons of the rat substantia nigra (pars compacta and pars reticulata): evidences for the existence of branched neurons. *Experimental Brain Research. Experimentelle Hirnforschung. Expérimentation Cérébrale* **32**, 409-422 (1978).

FIGURE LEGENDS

Figure 1: Transient changes in the basal ganglia output are reduced by ongoing population activity
A dataset of 599 single units was isolated from recording sessions with at least 8 simultaneously recorded units[17]. Electrodes were targeted to the substantia nigra and ventral tegmental region of mice trained to perform an auditory trace conditioning paradigm. (a) Spiking activity was z-scored, aligned to the onset of the conditioned stimulus (CS), and averaged for all units. (b) For each recorded unit the mean subtracted response ($RESP_{single}$) was computed as a function of the mean normalized activity prior to CS onset for the rest of the simultaneously recorded population ($PRE_{population}$; 7-20 units). Population data was binned, averaged, and fit with a sigmoid function (cyan line). (c) The correlation coefficient between $RESP_{single}$ and $PRE_{population}$ was computed for each session (n = 32). A histogram of all correlation scores is drawn with significant correlations (permutation test) indicated by filled gray bars. The correlation score of the entire population (-0.1) is indicated by a cyan triangle.

Figure 2: Light evoked activity of ChR2-expressing SNr GABA neurons in vitro
ChR2 was selectively expressed in SNr GABA neurons via two methods. Viral injection of AAV expressing *cre*-dependent ChR2-GFP transgene into SNr of a mouse line in which *cre*-recombinase was expressed under the glutamic acid decarboxylase (*Gad2*) promoter (a, *Gad2*-ChR2) and transgenic mouse line (*Thy1* Line18) which has ChR2 expression under the control of *Thy1* promoter (b, *Thy1*-ChR2), (a-b left: schematic of midbrain region with SN labeled and pipette representing injection target in (a), middle: midbrain coronal sections showing ChR2-GFP expression (green), right: two-photon image of ChR2-GFP positive SNr GABA neurons. *In vitro* wide-field illumination of midbrain slice (0.5 ms light pulse, 10 Hz, cyan arrows) reliably evoked action potentials in SNr GABA neurons in *Gad2*-ChR2 (c; n = 12/20 cells) and *Thy1*-ChR2 (d; n = 21/21 cells) mice, (c-d rater plot (upper) and cell-attached recording (lower) of a representative neuron from each mouse line showing evoked spiking over 5 trials repeating the same light stimulus. Quantification of light evoked spiking probability (e), latency (f) and standard deviation of the latency (jitter) (g) for a range of photostimulation durations recorded from both *Gad2*-ChR2 (red; n = 5 cells) and *Thy1*-ChR2 (green; n = 7 cells) mice. Representative light evoked ChR2-mediated inward current recorded at a range of membrane voltages (from -80 mV to +40 mV) from a single neuron recorded in either the *Gad2*-ChR2 (h) or *Thy1*-ChR2 (i) mouse. (j) Current-voltage relationship of light evoked currents recorded in either *Gad2*-ChR2 (red; n = 8 cells) or *Thy1*-ChR2 (green; n = 8 cells) mice.

Figure 3: The local inhibitory microcircuit of the SNr provides feedback gain control
(a) Schematic of the experimental configuration. 1-2 SNr GABA neurons were recorded from in the whole-cell current clamp configuration. Wide-field illumination of the slice (indicated by cyan circle) was used to photostimulate the SNr network. (b) Example recording from an individual SNr GABA neuron during light stimulation (upper cyan trace). Note the stereotyped membrane potential fluctuations during photostimulation (10 trials). (c-d) Example recordings from the same neuron recorded during 10 trials of stimulation ('Stim'; upper cyan trace) under control conditions (c; Cntrl; black) and following pharmacological blockage of inhibition via gabazine application (d; +Gbz; red) aligned to stimulus onset. Tick marks indicate spike times for 10 repetitions of the same light stimulus. Lower traces show the intracellular recording from the same neuron overlaid for all trials. (e) Raster plot of evoked spiking in control conditions (left) and in the presence of Gbz (right) for 4 blocks of 10 trails of increasing stimulus durations (4 ms, 8 ms, 12 ms, 20 ms; top to bottom) for a single neuron. (f) Raster plots of evoked spiking for 10 trials aligned to the onset of an 8 ms light stimulus for the population of neurons under control conditions (left) and in the presence of Gbz (right). (g) Normalized response across the population of neurons binned by stimulus duration and grouped by treatment (black, Cntrl and red, +Gbz). Significant effects on both stimulus duration and treatment condition were observed (Two-way ANOVA, $p<0.05$). Zero stimulus responses (open symbols) were estimated from the background firing rate. No significant difference was observed. (h) Full width half maximum (FWHM) of the peristimulus time histogram (PSTH)

for evoked spiking in control and following Gbz ($p<0.01$). (i) For paired recordings the percent inhibition of one neuron in the pair was plotted as a function of the percent inhibition of the other neuron for all stimulus conditions (black circles). A significant positive correlation was found and indicated by the solid black line ($p<0.01$; two tailed *t*-test).

Figure 3-figure supplemental 1: Direct comparison of responses elicited by optogenetic and natural stimulation

Peristimulus time histograms (PSTH) for a population of single units recorded from the SN of *Thy1*-ChR2 mice. (a) PSTHs were calculated for responses to optogenetic (LIGHT) stimulation through an optical fiber associated with a microwire array and (b) a 500 ms auditory stimulus (10 kHz pure tone, 500 ms duration) presented from a speaker positioned in front of the head-fixed animal (TONE). In both cases a strong transient response was observed and is evident in the mean PSTH (c-d). At the lower right panel the mean PSTH for TONE stimulation (filled black bars) and a scaled mean PSTH for LIGHT stimulation (red line) are overlaid (d).

Figure 3-figure supplemental 2: mIPSC amplitude in SNr GABA neurons

(a) Whole-cell recording from SNr neurons in control conditions (Cntrl) and following substitution of aCSF Ca^{2+} with 2 mM Sr^{2+} ($+Sr^{2+}$; V_h 30 mV). IPSCs were evoked via photostimulation of SNr collaterals (cyan) in slices from *Gad2*-ChR2 mice. Substitution of Ca^{2+} for Sr^{2+} was used to desynchronize release from SNr collateral synapses. (b-c) No difference between control sIPSCs and those enriched for SNr collaterals via desynchronized release was observed.

Figure 4: High background inhibition has little affect on tonic activity of SNr neurons

(a) Whole-cell recording of spontaneous IPSCs (sIPSCs) onto SNr neurons in control conditions (Cntrl; black trace) and following addition of tetrodotoxin (TTX) to isolate miniature events (+TTX; red trace, V_h 0 mV). (b) Cumulative histogram of IPSC amplitude in control conditions and following addition of TTX (n = 4 cells). (c) Box and whisker plot of IPSC amplitude for control and following addition of TTX. (d) Spiking output of SNr neurons following addition of high background excitation (upper) or inhibition (lower) via the dynamic clamp. (e) Summary data of change in firing rate of SNr neurons (n = 11 cells) following an increasing the relative frequency of inhibitory (red) or excitatory conductances (blue). (f) The slope of the change in firing rate as a function of change in conductance was significantly greater following increases in excitatory conductance compared to inhibitory conductance.

Figure 4-figure supplemental 1: Intrinsic, net inward currents and a positive slope conductance allows feedback gain control of SNr neurons

(a) Whole-cell recording of spontaneously spiking SNr neurons *in vitro* in the presence (upper black trace; Cntrl: AP5 & NBQX) and absence (lower red trace; +Gbz) of inhibition. Left shows tonic spiking and right shows ~20 action potential waveforms (grey) and average action potential waveforms (black, Cntrl; red, Gbz). (b) No significant change in spike frequency was observed following addition of Gbz (n = 11 cells; n.s. $p>0.05$, dotted red line represents unitary line). (c) Phase plot of example average spike waveform from an individual SNr neuron in control conditions (black trace) and following removal of inhibition (red trace), lower plot focuses on the perithreshold membrane potential dynamics. (d-e) Summary data of perithreshold and threshold slopes measured in control conditions and following pharmacological blockade of inhibition (+Gbz, n = 11 cells).

Figure 4-figure supplemental 2: Low release probability and sustained depression at feedback inhibitory synapse

(a) Representative IPSC during first second of photostimulation delivered at a range of frequencies (10,

20, 50, 100 Hz, indicated by labels at right of traces and cyan line) during whole-cell voltage clamp recordings from SNr GABA neuron. (b) Average peak IPSC amplitude, normalized to $IPSC_1$ (left axis; dark blue trace) and average tonic IPSC amplitude (right axis; grey trace) plotted as a function of stimulus number for 10, 20, 50 and 100 Hz photostimulation (*n* = 4 cells; shading represents SEM). (c) Peak Steady State (S.S.) IPSC ratio ($IPSC_{100}/IPSC_1$) and (d) S.S. tonic IPSC amplitudes ($IPSC_{100}$) plotted as a function of stimulation frequency (*n* = 4 cells). Error bars represent SEM.

Figure 5: Feedback inhibition has distinct biophysical properties from feed forward inhibition

(a) Schematic showing feedback nigral synapse (red arrow; *Gad2*-ChR2) and feed forward striatonigral synapse (blue arrow; *Drd1a*-ChR2) onto SNr GABA neurons. Synaptic properties of feedback inhibition were compared to feed forward inhibition to the SNr using photostimulation of ChR2 expressing SNr and striatal axons respectively. Wide-field 10 Hz photostimulation (cyan) to evoked activity of SNr GABA neurons in the *Gad2*-ChR2 mouse elicited large feedback IPSCs in SNr GABA neurons that were blocked with Gbz (b; *Gad2*-ChR2, *n* = 6 cells, P<0.001, paired two tailed *t*-test). Similarly, photostimulation of striatonigral afferents using *Drd1a*-ChR2 mouse evoked feed forward IPSCs in SNr GABA neurons that were blocked by Gbz (*n* = 5 cells, P<0.001, paired two tailed *t*-test). Histograms of measured IPSCs latency (d), rise time (e) and decay tau (f) for feed forward and feedback inhibition revealed feedback inhibition has significantly faster kinetics compared with feed forward inhibition. (g) Average IPSC amplitude as a function of stimulus duration for feed forward and feedback inhibition. (h) Fraction of $IPSC_1$ amplitude during a 10 Hz train of photostimulation for feed forward and feedback inhibition. For d-h; maroon traces represent data from *Gad2*-ChR2 mice measuring feedback inhibition, *n* = 15 cells; blue traces represent data from *Drd1a*-cre mice measuring feed forward inhibition, *n* = 18 cells; for d-h, P<0.001, paired two tailed *t*-test.

Figure 5-figure supplemental 1: Feedback inhibition provides fast, transient inhibition

Wide-field illumination of SN elicited large IPSCs in SNr GABA neurons recorded in *Gad2*-ChR2 (a, upper) and *Thy1*-ChR2 (b, upper) mice using a 10 Hz photostimulation protocol (cyan arrows). IPSCs were blocked with application of Gbz (a; *Gad2*-ChR2, *n* = 6 cells and b; *Thy1*-ChR2, *n* = 8 cells, lower, P<0.001 paired two tailed *t*-test). IPSC latency (c), rise time (d) and decay time (e) were not significantly different between recordings make in *Gad2*-ChR2 and *Thy1*-ChR2 mice. (f) Average IPSC amplitude as a function of stimulus duration evoked in *Gad2*-ChR2 mice was significantly reduced compared with IPSCs evoked in *Thy1*-ChR2 mice (P<0.05). (g) Fraction of $IPSC_1$ amplitude during a 10 Hz train of stimulation for neurons recorded from *Gad2*-ChR2 and *Thy1*-ChR2 mice. For c-g; maroon lines represent data from *Gad2*-ChR2 mice, *n* = 15 cells; green lines represent data from *Thy1*-ChR2 mice, *n* = 24 cells.

Figure 6: Circuit mapping of feedback inhibitory circuitry of SNr

(a, left) Schematic of the experimental configuration used for channelrhodopsin-assisted circuit mapping. Whole-cell voltage clamp recordings were obtained from SNr GABA neurons while a focus laser beam was scanned across the SNr to excite SNr neurons with high spatial resolution. (a, right) Postsynaptic responses to individual photostimulations (white) were aligned to the DIC image of the slice. Stimulation points are indicated by cyan. (b) Example of evoked IPSCs from a single recording with a histogram of IPSC latencies for all recordings. Evoked IPSCs were completely inhibited in the presence of Gbz (b, insert; *n* = 8 cells; P<0.001, paired two tailed *t*-test). (c) Cumulative histogram of response magnitude as a function of the distance between the stimulation site and recorded neuron in the *Thy1*-ChR2 (green) and *Gad2*-ChR2 (maroon) preparations. (d) Example of IPSC maps for two neurons. The dendritic arbor of each recorded neuron was reconstructed and transformed into the common SN reference frame (dotted line). For each neuron the center of mass (COM) of inhibition (COM_{IPSC}, filled diamond), COM of dendritic field (COM_{DEND}, filled square) and the isocontour of 50% inhibition (ISO_{IPSC}, colored line) were calculated. (e-f) The COM_{IPSC} was plotted as a function of the COM_{DEND} for each neuron recorded in coronal (e; *n* = 14 cells) and sagittal (f; *n* = 16 cells) sections and the correlation fit estimated (blue line).

Figure 6-figure supplemental 1: Light-evoked IPSCs result from perisomatic spiking

Calibration experiments where carried out to determine the resolution of photostimulation evoked spiking in individual SNr neurons in *Thy1*-ChR2 mice. (a) Cell-attached recordings from individual SNr neurons were made while a focused laser beam was scanned throughout a pre-defined grid of stimulation points spanning the SNr (see Methods). SNr neurons are tonically active, firing at ~10-40 Hz, thus to access which stimulation point evoked reliable spiking, spike traces were averaged over multiple (>3) trials, and voltage responses surrounding stimulation points were superimposed (a, upper). Voltage deflections which exceeded 50% of the maximum amplitude, and which fell within 1 standard deviation (1 SD) of the mean spike latency, were counted as generating reliable spiking. From this a corresponding color map of spiking reliability (scale bar, 0 = not reliable spiking, and 1 = reliable spiking) was generated (a, lower). (b) Whole cell recordings were then made from the same neuron to access photocurrent amplitude at each stimulation point using the same grid as in a. Cells were held at -70 mV to isolate ChR2 mediated photocurrent. Averaged photocurrents evoked at each stimulation point were superimposed (b, upper left) and shown with an expanded time scale (b, upper right) and as a corresponding color map of normalized peak amplitudes (b, right; scale bar, 0 = min amplitude, and 1 = max amplitude). For color maps in a & b blue dot indicates cell soma position, white scale bar represents distance between stimulation point. (c) The binned, normalized mean photocurrent response as a function of distance away from the soma (grey bars) and a fit to the binned probability of reliable spiking over the same distance for SNr GABA neurons (solid black line, *n* = 4 cells). All recordings were performed in the presence of synaptic transmission blockers. To test whether suprathreshold axonal stimulation of SNr collaterals could evoked synaptic transmission, SNr GABA neurons were voltage-clamped at V_h +20 mV to isolate IPSCs. Focused photostimulation throughout the SNr evoked IPSCs under control conditions (d, upper) and these were completely blocked following the addition of TTX (d, lower). (e) Population data showing TTX inhibition of IPSCs (e, *n* = 5 cells, P<0.001; paired two-tailed t-test). (f) For a subset of mapping experiments the latency to the detected IPSC is plotted as a function of distance from soma of the stimulation site. Although the spread is rather large due to variations in latency of evoked spikes by ChR2 positive SNr neurons, there is significant slope towards added propagation delays of ~0.5 ms per 1 mm of stimulation distance. This corresponds to roughly 2 m/s conduction velocities, which is comparable to previously obtained estimates (1.7 m/s) in rats [67].

Figure 7: Intranigral inhibition is poorly predicted by the organization of the striatonigral pathway

Neurons in the dorsal striatum of *Drd1a*-cre x *Thy1*-ChR2 double transgenic mice were infected with cre-dependent AAV that drove the expression of a red fluorescent protein to label striatonigral axons (tdTomato). Bright-field images of the fluorescent axons in the SN were used to estimate the location of labeled axons (a, bottom layer). Estimates of the density of axonal labeling were produced by extracting the axon contour (quartiles indicated by gray line thickness) and compared with the localization of local inhibitory input (thresholded at 20% of maximum response) for multiple neurons recorded in the same slice (a, upper 3 layers). Individual postsynaptic neurons with proximal dendritic arbors reconstructed are shown in shades of red. The approximate border of the SN is indicated (cyan dashed line). (b) The correlation in spatial maps of IPSC amplitudes were computed for all pairwise comparisons between neurons recorded in the same slice (*n* = 10 slices; *n* = 36 cells) as a function of the distance between somata. Gray circles are individual correlations, red circles are binned means with standard errors, and solid red line is an exponential fit. (c) For each slice the correlation between a spatial map of IPSC amplitudes and the axonal density map is shown as a function of the distance between the soma of the recorded neuron and the center of mass of the axon projection. (d) For all slices the maximum intensity contrast (see Methods) for the axonal labeling was overlaid with the location of all recorded somata (red circles). The angle and distance to the center of mass of the spatial maps of IPSC amplitudes are indicated by the red arrows. An example projection field from a single infection of the dorso-medial striatum is shown in dark cyan.

Figure 7-figure supplemental 1: Mapping striatonigral axonal terminal fields
Focal injections of a cre-dependent AAV expressing tdTomato was targeted to the striatum of *Drd1a*-cre x *Thy1*-ChR2 mice to allow both labeling of a subset of striatonigral projecting axonal and subsequent CRACM of the local inhibitory network within the SNr (*n* = 5 animals). Example slices from 4 mice with striatal injections (upper) and their corresponding axonal terminals in the SNr (lower).

Figure 7-figure supplemental 2: Anatomical organization of the striatonigral pathway
(a) Two *cre*-dependent AAVs driving the expression of different fluorescent protein transgene (indicated in top labels) was injected into the medial (green) and lateral (red) aspect of the striatum in *Drd1a*-cre mice. (b) Axonal fibers were found in the SN. The axon termination zones showed strong fluorescence and were largely non-overlapping for injections at the striatal extrema.

Figure 8: Potent and diffuse intranigral inhibition in vivo
(a) Schematic of experimental configuration used for *in vivo* recordings. An optical fiber was affixed to one shank of a silicon probe electrode array. The array was lowered into the SN of awake, head-fixed mice. (b) Raster plots of responses to light stimulation for two example single units isolated from such recordings. Spikes are indicated by vertical hash marks, colored and sorted by stimulus duration. Mean PSTHs are shown in lower panels and the average waveform (+/- 1 s.d.) are shown in the insets. Some units (e.g., s06u01) exhibited direct excitation by photostimulation followed by suppression. While other units (e.g., s03u21) located at a more eccentric position on the array exhibited a delayed (one 5 ms PSTH bin) suppression of firing. (c) The distribution of average firing rates was very similar for single units isolated *in vivo* (gray bars) and on cell spiking rates observed *in vitro* (open bars). Directly excited units (red bars) and units exhibiting inhibition below baseline (open cyan bars) are plotted as a function of baseline firing rate. (d) The mean response magnitude for units exhibiting short latency activation (red) and the most inhibited quartile of the population (cyan) are plotted as a function of stimulus duration. (e) The spatial arrangement of sites at which direct excitation (red) or inhibition below baseline (cyan) was observed. Left, individual shanks of the silicon probe array are shown as light gray lines and the shank to which the optical fiber was affixed is shown in darker gray. The position of individual recording sites are represented as black dots. Every significant excitatory and/or inhibitory response is represented as a triangle or circle, respectively. Scale bar: 200 µm, 5 z*ms. The diameter of the symbol reflects the magnitude of the response to stimulation for stimuli of 20 (upper) and 50 (lower) ms stimuli. Middle, a maximum intensity projection for direct excitation (red) and inhibition (blue). Scaling of maximal value is shown in lower left. Right, a cumulative histogram of response magnitude as a function of distance from the focus of excitation (most strongly activated site on the shank with associated optical fiber). Distance calculated based upon 200µm site spacing on the silicon probe array.

Figure 8-figure supplemental 1: Feedback inhibition shapes SNr output in Thy1-ChR2 transgenic mice
(a) Schematic of experimental configuration used for *in vitro* recordings. (b) The population response of recorded projection neurons in response to photostimulation of varying durations was sorted by the normalized magnitude of the response (cyan = -1, red = +1) for control (Cntrl) conditions. (c) The normalized difference of responses between stimulation under control conditions and stimulation in the presence of gabazine (Gbz). (d) Schematic of experimental configuration used for *in vivo* recordings. (e) Normalized PSTHs for single units with baseline firing greater than 9 Hz (*n* = 147 cells) were aligned to stimulus onset. Colors as in b, inhibition and excitation normalized independently. (f) Mean PSTHs were calculated for the population of neurons with a dominant excitatory response (left, see methods) for *in vitro* (black) and *in vivo* recordings (36% of population, red) or a dominant inhibitory response (right, see methods) for *in vitro* (black) and *in vivo* recordings (13% of population, cyan). (g) Raster plots and boxcar averages are shown from example neurons. Examples were selected by finding the single unit PSTH with

the highest correlation to the population PSTH for excitation dominant (left) and inhibition dominant (right) populations

Figure 9: Schematic Summary of proposed mechanism for divisive gain control in a circuit lacking interneurons.

(a) Schematic of the canonical basal ganglia circuit with detail showing the anatomical basis for intrinsic feedback control of the basal ganglia output via the intrinsic microcircuitry of the substantia nigra. (b) Comparison of candidate mechanisms for gain control described in microcircuits with interneurons (*e.g.* Silver, 2010) with the mechanism for divisive gain control in the substantia nigra (a circuit thought to lack interneurons) described here.

Figure 1

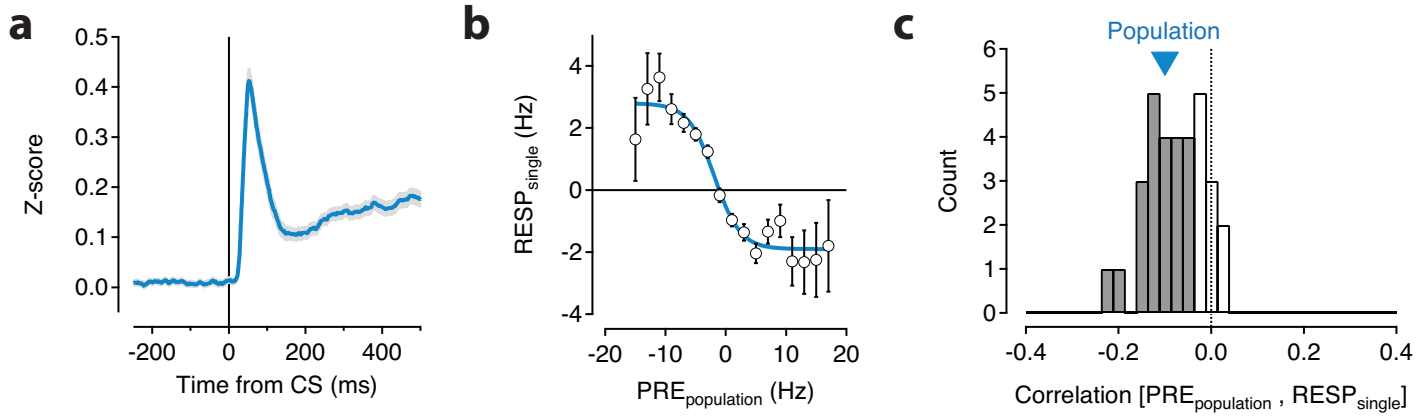
a
Z-score
0.5
0.4
0.3
0.2
0.1
0.0
-200
0
200
400
Time from CS (ms)
b
RESP$_{single}$ (Hz)
4
2
0
-2
-4
-20
-10
0
10
20
PRE$_{population}$ (Hz)
c
Population
Count
6
5
4
3
2
1
0
-0.4
-0.2
0.0
0.2
0.4
Correlation [PRE$_{population}$, RESP$_{single}$]

Figure 2

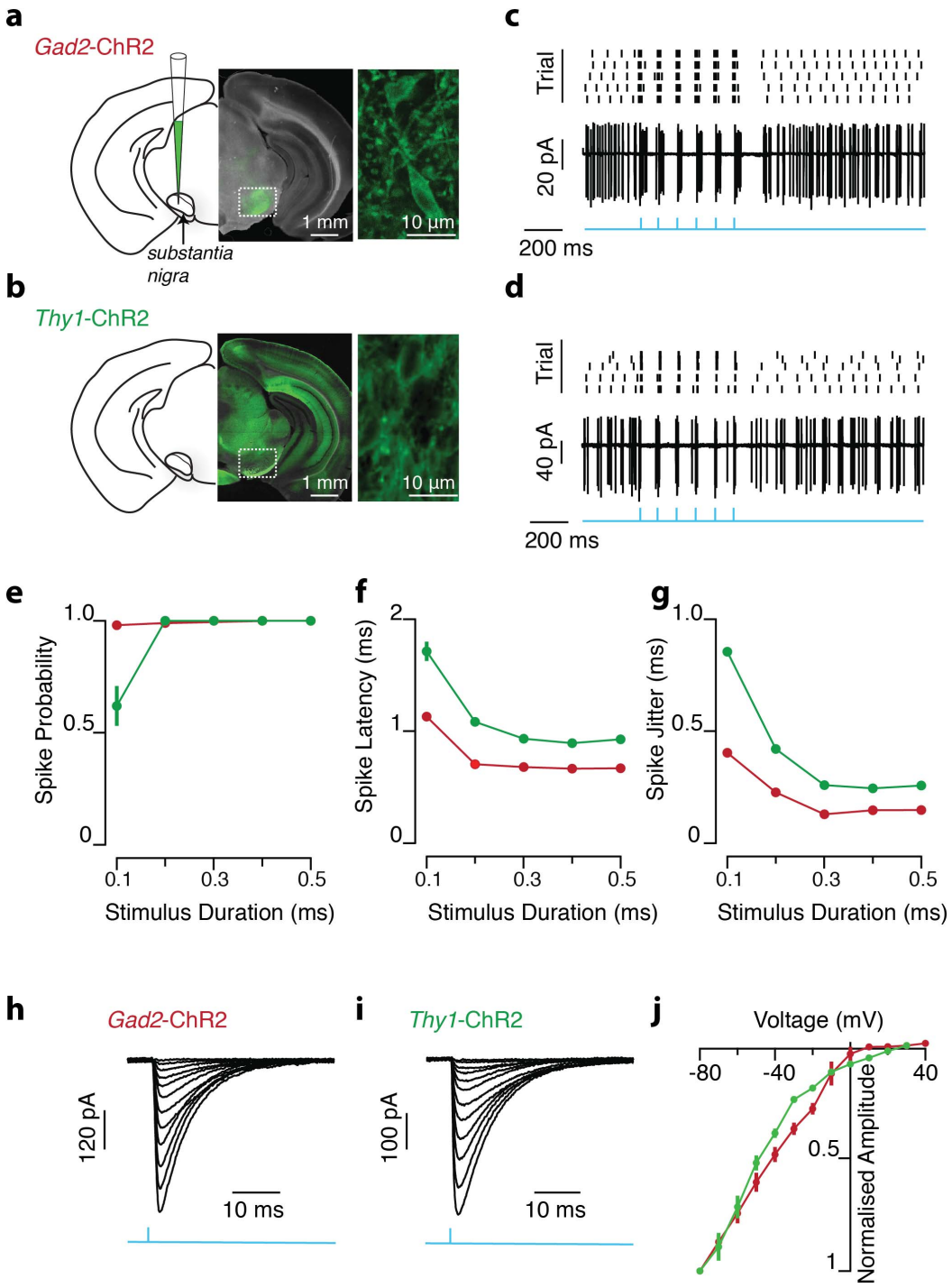
a
Gad2-ChR2
1 mm
10 µm
substantia nigra
b
Thy1-ChR2
1 mm
10 µm
c
Trial
20 pA
200 ms
d
Trial
40 pA
200 ms
e
Spike Probability
1.0
0.5
0
0.1
0.3
0.5
Stimulus Duration (ms)
f
Spike Latency (ms)
2
1
0
0.1
0.3
0.5
Stimulus Duration (ms)
g
Spike Jitter (ms)
1.0
0.5
0
0.1
0.3
0.5
Stimulus Duration (ms)
h
Gad2-ChR2
120 pA
10 ms
i
Thy1-ChR2
100 pA
10 ms
j
Voltage (mV)
-80
-40
40
0.5
1
Normalised Amplitude

Figure 3

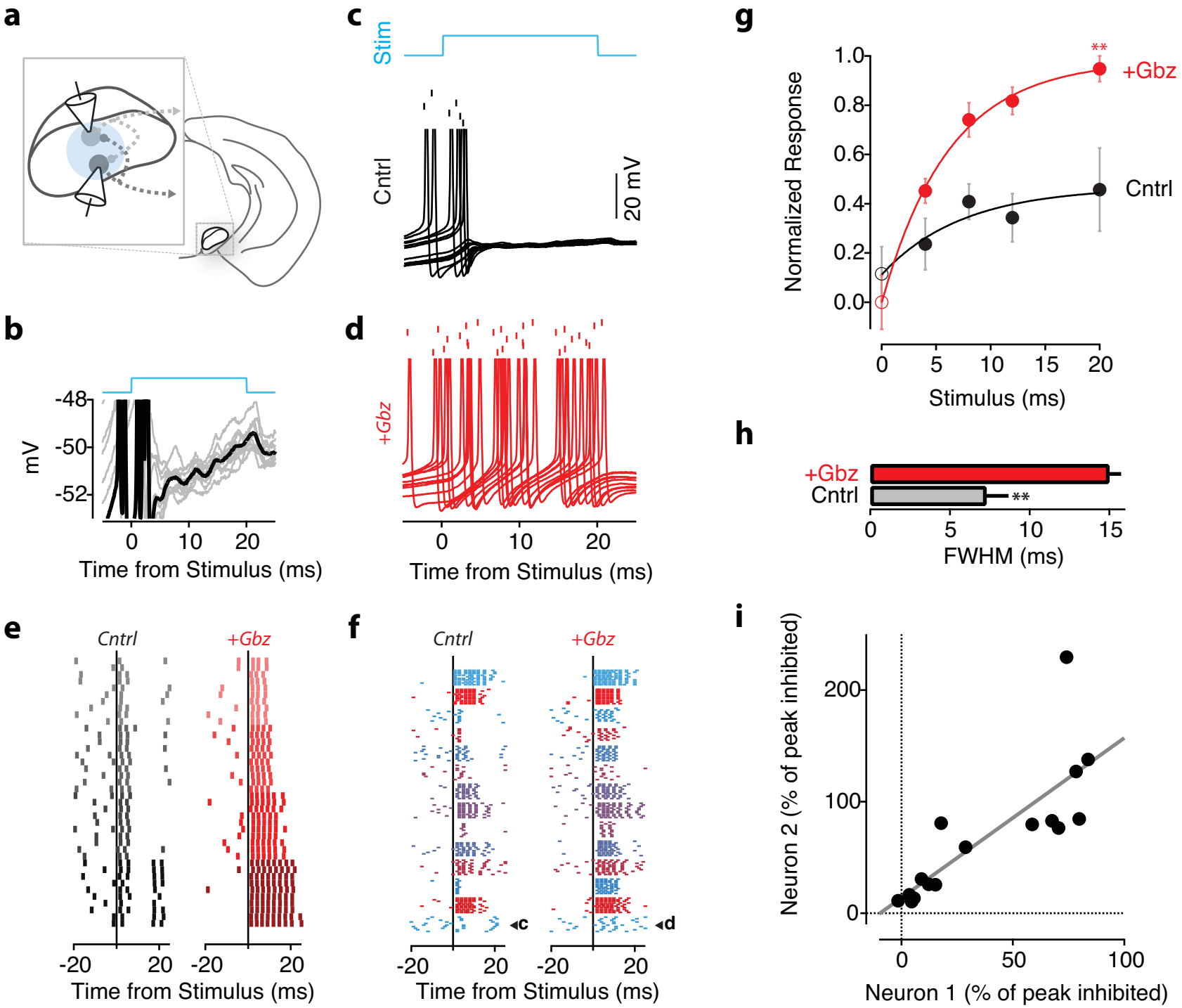
a
b
-48
-50
-52
mV
0
10
20
Time from Stimulus (ms)
c
Stim
Cntrl
20 mV
d
+Gbz
0
10
20
Time from Stimulus (ms)
e
Cntrl
+Gbz
-20
20
-20
20
Time from Stimulus (ms)
f
Cntrl
+Gbz
◂c
◂d
-20
20
-20
20
Time from Stimulus (ms)
g
1.0
0.8
0.6
0.4
0.2
0.0
Normalized Response
**
+Gbz
Cntrl
0
5
10
15
20
Stimulus (ms)
h
+Gbz
Cntrl
**
0
5
10
15
FWHM (ms)
i
200
100
0
Neuron 2 (% of peak inhibited)
0
50
100
Neuron 1 (% of peak inhibited)

Figure 4

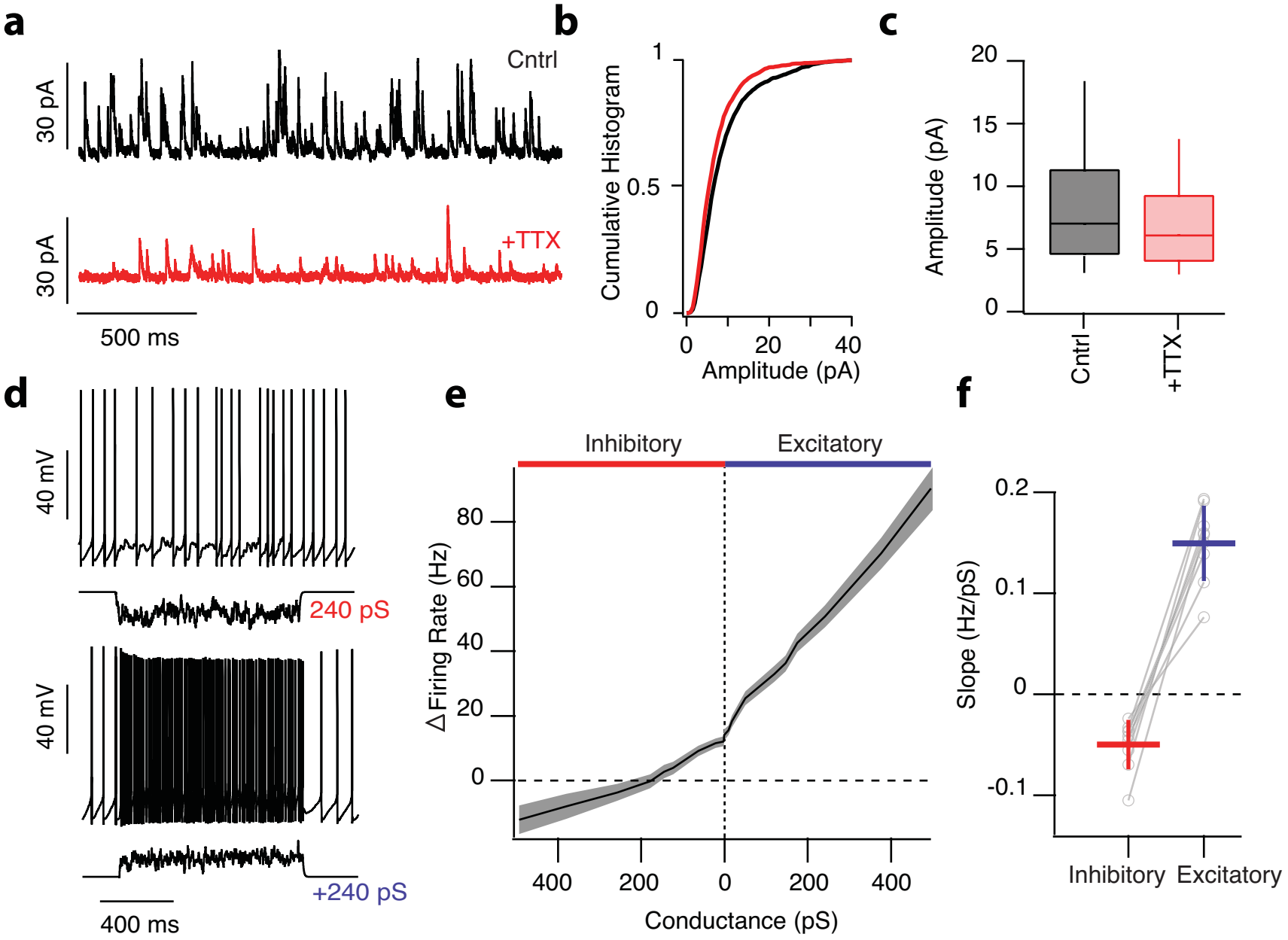
a
Cntrl
30 pA
+TTX
30 pA
500 ms
b
Cumulative Histogram
1
0.5
0
0
20
40
Amplitude (pA)
c
Amplitude (pA)
20
15
10
5
0
Cntrl
+TTX
d
40 mV
240 pS
40 mV
+240 pS
400 ms
e
Inhibitory
Excitatory
ΔFiring Rate (Hz)
80
60
40
20
0
400
200
0
200
400
Conductance (pS)
f
Slope (Hz/pS)
0.2
0.1
0
-0.1
Inhibitory
Excitatory

Figure 5

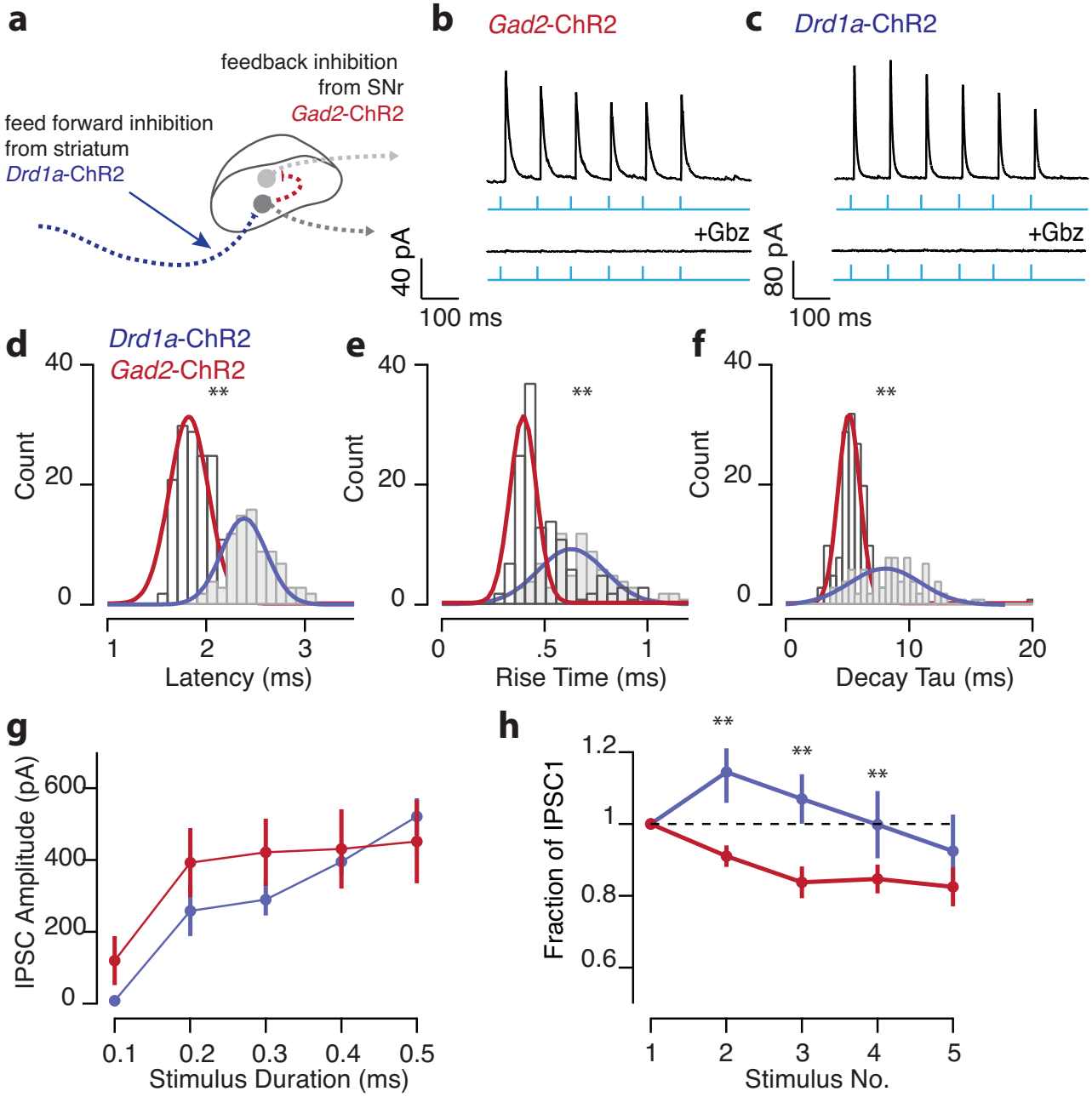
a
feedback inhibition
from SNr
Gad2-ChR2
feed forward inhibition
from striatum
Drd1a-ChR2
b
Gad2-ChR2
+Gbz
40 pA
100 ms
c
Drd1a-ChR2
+Gbz
80 pA
100 ms
d
Drd1a-ChR2
Gad2-ChR2
Count
Latency (ms)
e
Rise Time (ms)
f
Decay Tau (ms)
g
IPSC Amplitude (pA)
Stimulus Duration (ms)
h
Fraction of IPSC1
Stimulus No.

Figure 6

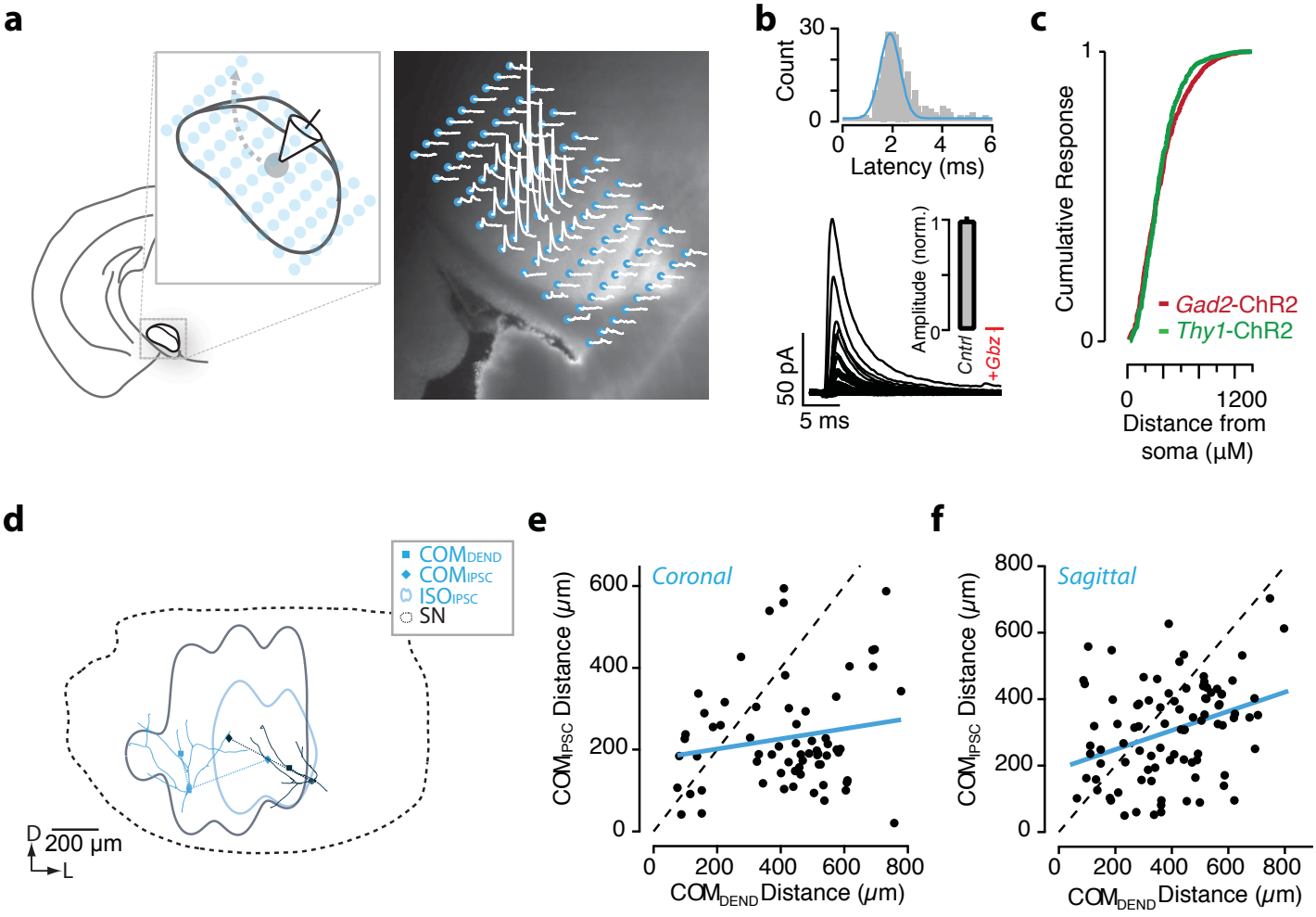
a
b
Count
30
0
0
2
4
6
Latency (ms)
50 pA
5 ms
Amplitude (norm.)
1
0
Cntrl
+Gbz
c
Cumulative Response
1
0
Gad2-ChR2
Thy1-ChR2
0
1200
Distance from soma (µM)
d
COMDEND
COMIPSC
ISOIPSC
SN
D
200 µm
L
e
Coronal
COMIPSC Distance (µm)
600
400
200
0
0
200
400
600
800
COMDEND Distance (µm)
f
Sagittal
COMIPSC Distance (µm)
800
600
400
200
0
0
200
400
600
800
COMDEND Distance (µm)

Figure 7

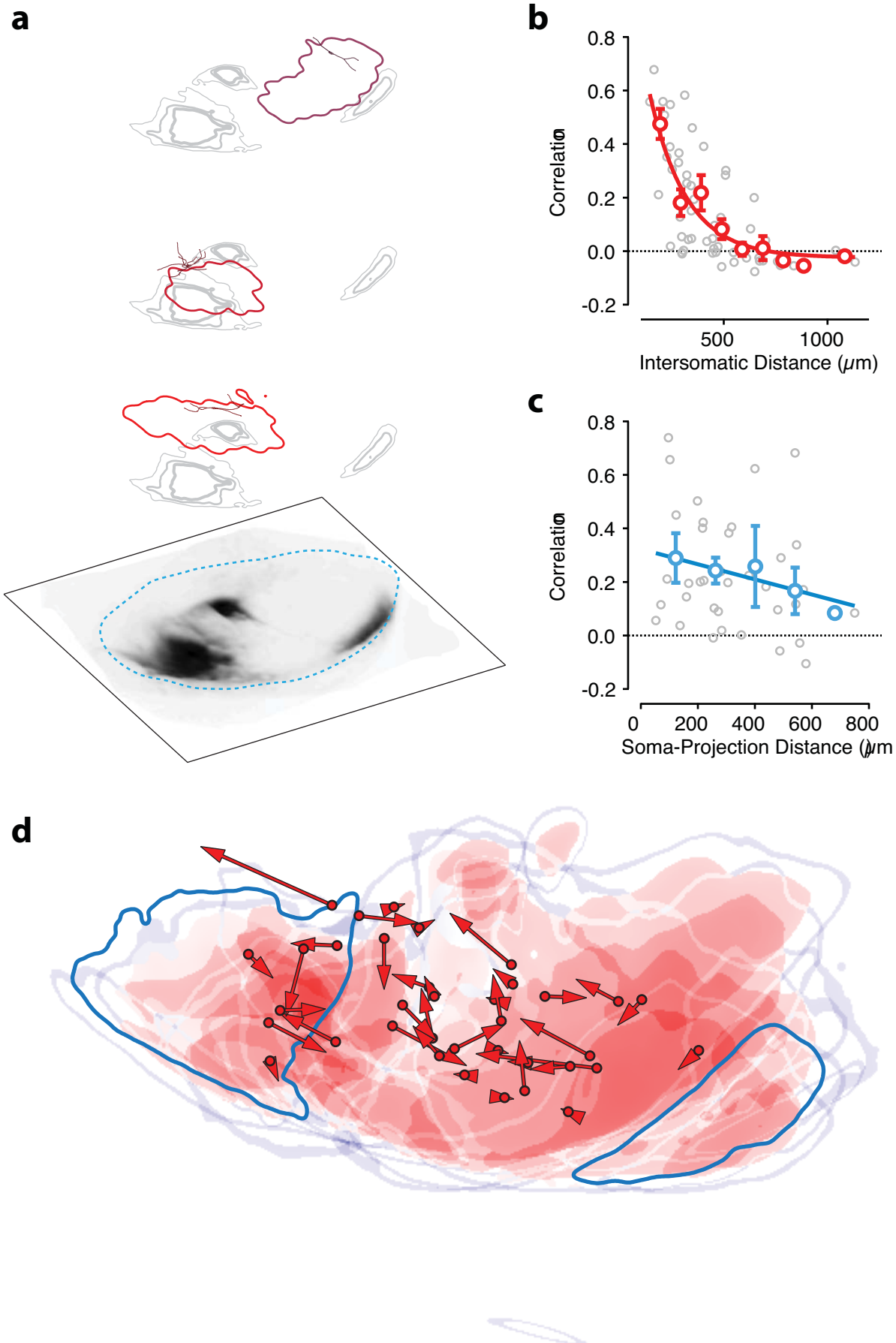
a
b
0.8
0.6
0.4
0.2
0.0
-0.2
Correlation
500
1000
Intersomatic Distance (μm)
c
0.8
0.6
0.4
0.2
0.0
-0.2
Correlation
0
200
400
600
800
Soma-Projection Distance (μm
d

Figure 8

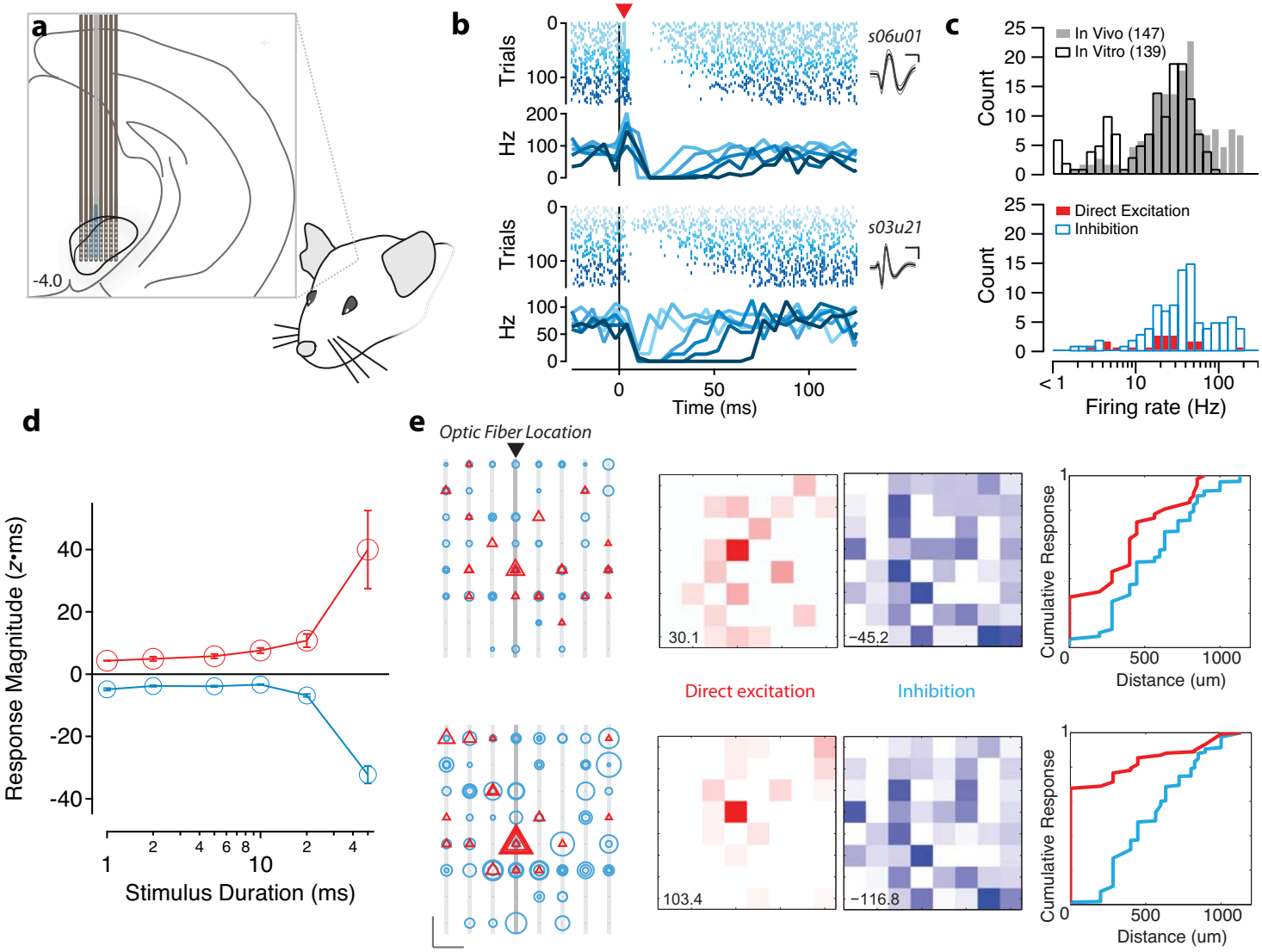
a
-4.0
b
Trials
Hz
s06u01
s03u21
Time (ms)
c
In Vivo (147)
In Vitro (139)
Count
Direct Excitation
Inhibition
Firing rate (Hz)
d
Response Magnitude (z•ms)
Stimulus Duration (ms)
e
Optic Fiber Location
30.1
−45.2
103.4
−116.8
Direct excitation
Inhibition
Cumulative Response
Distance (um)

Figure 9

a

Anatomical Basis

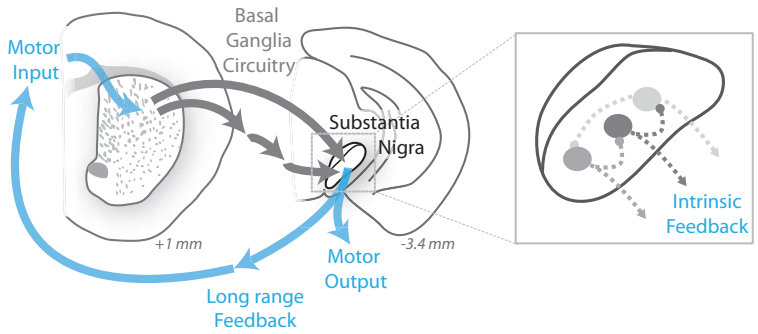

b

Function / Mechanism

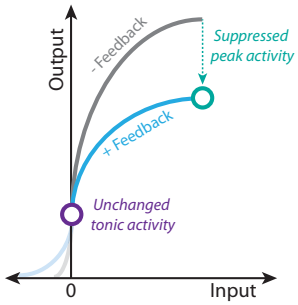

Proposed mechanisms in circuits with interneurons	*Our proposed mechanism in a circuit lacking interneurons*
1. Distinct plasticity at excitatory and inhibitory synapses *2. Input nonlinearities in projection neuron but not interneuron* *3. Proportional change in excitation and inhibition*	*1. Collect inputs from broad area (i.e. number of neurons)* *2. Robust inhibition from correlated activity* *3. Proportional recruitment of inhibition* *4. Lack of spatial overlap with feed forward input*
1. Lack of significant disynaptic inhibition (e.g. lack of baseline activity or presynaptic inhibition) *2. Balanced excitation and inhibition*	*1. Weak unitary connections with low release probability* *2. Asynchronous input due to variable tonic firing* *3. Relative insensitivity to tonic inhibition*